The Potential of ALOS-2 and Sentinel-1 Radar Data for Soil Moisture Retrieval With High Spatial Resolution Over Agroforestry Areas, China

Huizhen Cui, Lingmei Jiang, *Member, IEEE*, Simonetta Paloscia, *Fellow, IEEE*,
Emanuele Santi, *Senior Member, IEEE*, Simone Pettinato, *Member, IEEE*, Jian Wang,
Xiyao Fang, and Wanjin Liao

Abstract— Synthetic aperture radar (SAR) sensors, such as Advanced Land Observing Satellite-2 (ALOS-2) and Sentinel-1, provide significant opportunities for soil moisture content (SMC) retrieval with relatively high spatial resolutions (10∼30 m). In this work, an artificial neural network (ANN) SMC retrieval algorithm combined with the water cloud model, the advanced integral equation model, and the Oh model database was proposed. The SAR copolarization backscatter, the local incidence angle (LIA), and the normalized difference vegetation index were used in input vectors for the ANN algorithm for the retrieval and mapping of the ALOS-2 and Sentinel-1 SMC at a 30-m resolution. The results of the comparison between the SMC retrievals and the measured SMC show that Sentinel-1 and ALOS-2 SMC retrievals with high accuracy correspond to low-vegetation areas (crop, grass, and shrub), with a root mean square error (RMSE) of 0.021 and 0.033 cm³/cm³, respectively. ALOS-2 SMC retrievals provide higher accuracy (RMSE = 0.076 cm³/cm³) than Sentinel-1 SMC retrievals at high vegetation (e.g., forest). However, it remains challenging for soil moisture retrieval in forest land. The C-band and L-band SMC retrievals have higher RMSE (up to 0.047 cm³/cm³) at low incidence angle (<20°) and high incidence angle (>50°). In addition, by considering the impact of rainfall on the SMC, it appears that the Sentinel-1 and ALOS-2 SMC have a good response to the rainfall events. Finally, the results of the comparison between the SMC retrievals and the Soil Moisture Active Passive (SMAP) L2 SMC product show that the correlation coefficients between Sentinel-1, ALOS-2, and SMAP are higher in September when the vegetation is drying than in July when the vegetation is growing.

Index Terms— Advanced Land Observing Satellite-2 (ALOS-2), agroforestry area, artificial neural network (ANN), Sentinel-1, soil moisture content (SMC).

I. INTRODUCTION

SOIL moisture content (SMC) is one of the most active parameters in the process of energy and water interchange between the land surface and atmosphere, and it is also a key variable for several applications in hydrological processes, bioecological processes, and biogeochemical processes [1]. High-spatial-resolution measurements of SMC have widespread applications in agricultural irrigation, hydrological modeling, and meteorological climate forecasting [2]. Remote sensing techniques, with the launch of new sensors with improved performances in terms of accuracy and spatial resolution, provide a flexible alternative to capturing the SMC at regional and global scales, in particular using optical/thermal infrared and microwave sensors [3], [4]. Optical/thermal infrared sensors (TIRSs) are affected by weather conditions (e.g., cloud and rainfall), which makes them encounter difficulties in estimating the SMC continuously over space and time. Passive microwave satellites can provide a long-term series of SMC datasets for large areas. However, the satellites, which include FengYun-3B/C/D (FY-3B/C/D), Advanced Microwave Scanning Radiometer-2 (AMSR2), Soil Moisture and Ocean Salinity (SMOS), and Soil Moisture Active Passive (SMAP), have a coarse spatial resolution (25∼36 km), which is limiting for many applications that require high spatial resolution. Active microwave remote sensing instruments, such as synthetic aperture radar (SAR) sensors, can provide observations at higher spatial resolutions and show rather high sensitivity to vegetation biomass and SMC, especially at low microwave frequencies (i.e., the C- and L-bands) [1], [5].

Microwave sensors that operate from the P- to L-bands are more sensitive to variations in the SMC of bare and vegetated soils, which provides information for consistent soil layers [6]–[8]. However, most radar systems operate mainly at the C-band (e.g., RADARSAT and ENVISAT) and X-band

(e.g., COSMO-SkyMed and TerraSAR-X). Although some preliminary studies have indicated some sensitivity of X-band signals to the SMC [9], this frequency does not represent the optimal option for SMC retrieval. The current satellite missions of Sentinel-1 with C-band SAR and Advanced Land Observing Satellite-2 (ALOS-2) with L-band SAR provide more opportunities for SMC retrieval at a high spatial resolution. At present, there are many studies that focus on SMC retrieval using Sentinel-1 data [10]–[14], but there is limited research on SMC retrieval using ALOS-2 [15], [16], which is mainly due to the scarce worldwide coverage and lack of image availability. Thus, the performance of ALOS-2 SAR to retrieve SMC requires further validation. At the same time, to obtain the highest accuracy and spatial resolution of the SMC product in the future, the potential of Sentinel-1 (C-band SAR) and ALOS-2 (L-band SAR) to retrieve SMC under different land surface conditions should be compared and investigated with a more in-depth approach.

In the process of SMC retrieval, both the surface roughness and vegetation cover have a significant effect on the radar signal, and therefore, they are the key issues to be considered. Some backscattering models have been developed to describe the scattering mechanisms of bare soil and vegetation surfaces. For bare soil, the most commonly adopted models are the integral equation model (IEM) [17], the advanced IEM (AIEM) [18], and the Oh model [19]. These models allow for simulation of the radar signals, SMC, and soil roughness under specific soil conditions. Most studies use mainly vegetation models combined with bare soil models to simulate the backscattering in the vegetation-covered areas. The most popular models are the water cloud model (WCM) [20] and the Michigan Microwave Canopy Scattering (MIMICS) model [21]. The input parameters of the MIMICS model are complex and sometimes difficult to obtain, which limits the widespread application of this model. WCM requires a few input parameters, and it is also simpler in implementation; as a result, it is more widely used in SMC retrieval [15], [22], [23].

Based on SAR images and these models, many SMC retrieval algorithms have been widely implemented for different land surfaces in the past [9], [15], [16], [24], which mainly includes change detection approaches [10], [14], [25], [26], physical models [1], [5], [27], [28], and statistical methods [11], [30]–[32]. However, these retrieval algorithms are mainly applied to bare soil, sparsely vegetated surfaces, cropland, and grassland, whereas limited studies have been conducted for dense vegetation areas, especially in agroforestry areas. Agroforestry areas are the typical pattern of shelterbelts and cropland in China's Three-North Shelter Forest Program [32]. A high-spatial-resolution SMC estimation is important for estimating carbon emissions and carbon storage and identifying the influence of water circulation in agroforestry areas [3].

Over the last two decades, among the statistical approaches for retrieving SMC, artificial neural networks (ANNs) [23], [24], [33], [34] have been widely used since they have the power to retrieve the complex, dynamic, and nonlinear patterns from the data, and therefore, they are widely applied in many land surface parameter retrieval studies

that use remote sensing data [35]–[37]. In SMC retrieval, the ANN algorithm gives a better compromise in terms of the accuracy, computational time, and criticality compared with statistical algorithms based on Bayes' theorem, iteration algorithms based on the Nelder–Mead minimization method, and linear regression algorithms [24]. Subsequently, the potential of machine learning methods for SMC retrieval was investigated [22]–[24], [37], and the effectiveness of these methods in solving SMC retrieval problems has been proved, mainly using C-band or X-band SAR images of bare soil, grassland, and cropland.

Therefore, due to the complexity of the land surface in the agroforestry area and considering the ease of implementation of ANNs in retrieving SMC, this article describes an algorithm based on ANNs to retrieve SMC from C-band and L-band SAR. Since it is well-known that one of the critical points of ANNs is the training phase, in this algorithm, we used a training set derived from model backscattering coefficient simulations obtained from the WCM, AIEM, and Oh models that account for different land surface types and radar characteristics.

This work aims at investigating the potential of Sentinel-1 and ALOS-2 SAR data for the estimation of SMC and developing an SMC retrieval algorithm at a high spatial resolution over agroforestry areas. Currently, the SMC validation is mainly based on measured ground data [10], [22], [23], [38]. However, the spatial representation of the measured sites is limited. To better validate the retrieval results, in addition to the ground measured data, the remote sensing product SMAP L2 radiometer/radar SMC is used to intercompare the Sentinel-1 and ALOS-2 SMC estimates. The proposed approach for the retrieval of SMC in agroforestry areas is based on an ANN algorithm trained by using WCM combined with AIEM and Oh model simulations. First, we generated a simulated database based on the calibrated WCM combined with AIEM and the Oh model. Half of the total data of the simulated parameters were used for training the ANN, and the other half of the simulated data was used for the validation of the algorithm. Second, Sentinel-1 and ALOS-2 SAR backscattering coefficient, local incidence angle (LIA), and normalized difference vegetation index (NDVI, derived from Sentinel-2 and Landsat 8) are input to the ANN to retrieve the SMC. Finally, Sentinel-1 and ALOS-2 SMC retrievals were validated based on the ground measurements and compared with the SMAP L2 SMC product. This article is organized as follows. Section II presents the study area and database. Section III describes the data analysis and proposed methodology. Section IV presents and discusses the result of algorithm validation and SMC maps. Finally, the conclusions are summarized in Section V.

II. STUDY AREA AND DATASET

The study was conducted in the Genhe watershed of China, which is mainly an area of agricultural and forestry ecotones. In the following, only a brief description of this study area is given because it is described in detail in other papers [3], [39]. The data used in this article are mainly composed of *in situ* observations of SMC, soil temperature, surface
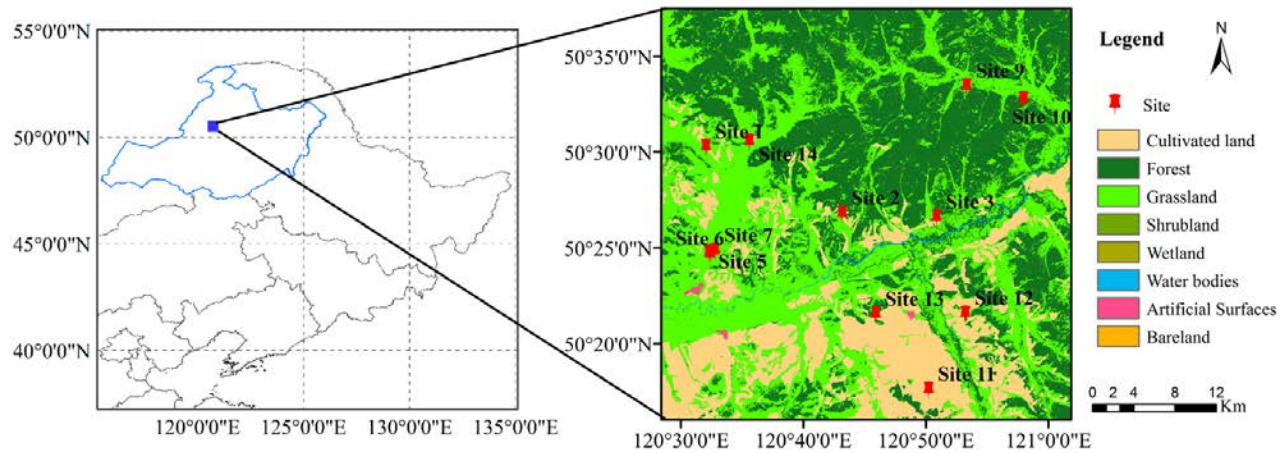
This article has been accepted for inclusion in a future issue of this journal. Content is final as presented, with the exception of pagination.

CUI *et al.*: POTENTIAL OF ALOS-2 AND SENTINEL-1 RADAR DATA FOR SOIL MOISTURE RETRIEVAL 3

Fig. 1.   Land cover map in the Genhe watershed (from GlobeLand30, http://www.globallandcover.com/).

roughness and soil texture, Sentinel-1 and ALOS-2 SAR data, GlobeLand30 land cover information, and NDVI. Considering the Genhe watershed with frequent cloud weather and the quality of the optical data, two optical satellites, namely, Sentinel-2 and Landsat 8, are selected to derive the NDVI and complement each other under cloudless conditions. To maintain the consistency of the spatial resolution, the Sentinel-1, ALOS-2, and Sentinel-2 observations in this article were all sampled at 30 m (by taking the average value of 10-m pixels, inside each 30-m pixel).

A. In Situ Data

The Genhe watershed is the northernmost and coldest area in Inner Mongolia, and it is mainly a zone of interspersed agriculture, grassland, and forestry. As shown in Fig. 1, the SMC and soil temperature observation network were deployed on both sides of the Genhe watershed (50.16°–50.66° N, 120.5°–121.0° E), and the detailed information on the sites is shown in Table I. The SMC and soil temperature were continuously measured via the Em50 data collection system with EC-5TM probes (Decagon Devices, Inc., Washington, DC, USA) from October 2013 to September 2019. Considering the penetrability of the C-band and the L-band in complex land surfaces over the Genhe watershed, the average SMC and soil temperature observations from top 3- and 5-cm layers were selected to be used in this work. Soil surface roughness was measured by a pin profiler at each site. The surface roughness measurements of the root mean square height and correlation length in the study area were approximately 0.8~1.5 and 5~15 cm, respectively. Vegetation height was derived from *in situ* measurements at complicated observations and multiparameter land information constructions on allied telemetry experiment (COMPLICATE) [40] and Genhe watershed observation network [39]. Soil texture was measured in the laboratory with soil samples by the cutting ring method in the field. The topsoil texture of this area is mainly composed of silt (50%~54%), sand (6%~9%), and clay (39%~44%).

B. SAR Data

The local overpass time and temporal resolution of the Sentinel-1 and ALOS-2 SAR sensors are different. To better

TABLE I
INFORMATION ON THE SITES IN THE STUDY AREA

Site name	Lon. (deg.)	Lat. (deg.)	Alt. (m)	Land cover	Time(Day/ Month/Year)
Site 1	120.522	50.505	705	Grass	07/10/2013-
Site 2	120.711	50.451	699	Larix gmelinii	10/10/2013-
Site 3	120.840	50.450	628	Shrub, Birches	06/10/2013-
Site 5	120.531	50.413	628	Grass, Shrub	07/10/2013-
Site 6	120.533	50.412	673	Grass	07/10/2013- 09/10/2015
Site 7	120.539	50.415	792	Grass	07/10/2013- 19/09/2015
Site 9	120.876	50.565	705	Birch forest	21/04/2015-
Site 10	120.954	50.555	728	Larix gmelinii	21/04/2015- 02/10/2015
Site 11	120.836	50.300	724	Shrub, Birches	10/10/2015-
Site 12	120.883	50.367	651	Shrub	10/10/2015-
Site 13	120.761	50.364	754	Birch forest	10/10/2015- 10/05/2017
Site 14	120.581	50.511	731	Birch forest	09/10/2015-

compare the retrieval results of the Sentinel-1 and ALOS-2 SAR sensors, data with similar overpass times of the two satellites are screened out within the period from 2015 to 2016 (see Table II). Cui *et al.* [3] have shown that the soil surface in the Genhe watershed is frozen at the beginning of November and thawed at the beginning of April. The state of the SMC is complicated under frozen conditions, due to low dielectric constant values of frozen soils, and thus, this work was conducted for the unfrozen season only, by removing data that corresponded to frozen dates from the analysis. The satellite passes that correspond to unfrozen conditions are shown in Table II with the mark *.

1) Sentinel-1: The Sentinel-1 mission is the European Radar Observatory for the Copernicus joint initiative of the European Commission and the European Space Agency. A C-band (5.405 GHz) SAR is aboard Sentinel-1, and it provides the dual-polarization capability. Sentinel-1 comprises a constellation of two polar-orbiting satellites: Sentinel-1A (launched on

TABLE II
SAR DATA WITH SIMILAR OVERPASS TIME (*UNFROZEN CONDITIONS)

Sensor	Date	Sensor	Date
Sentinel-1A	Feb 17, 2015	ALOS-2	Feb. 13, 2015
Sentinel-1A	Jul 18, 2015*	ALOS-2	Jul. 17, 2015*
Sentinel-1A	Sep 28, 2015*	ALOS-2	Sep. 25, 2015*
Sentinel-1A	Dec 9, 2015	ALOS-2	Dec. 4, 2015
Sentinel-1A	Feb 7, 2016	ALOS-2	Feb. 12, 2016
Sentinel-1A	Jul 12, 2016*	ALOS-2	Jul. 15, 2016*
Sentinel-1A	Sep 22, 2016*	ALOS-2	Sep. 23, 2016*
Sentinel-1B	Dec 9, 2016	ALOS-2	Dec. 2, 2016

TABLE III
DATASETS INFORMATION (SR: SPATIAL RESOLUTION; RES: RESAMPLING RESOLUTION)

Datasets	Acquisition date	Parameter	SR (m)	RES (m)
Sentinel-1	Jul 18, 2015 Sep 28, 2015 Jul 12, 2016 Sep 22, 2016	backscattering coefficient (VV, VH)	10	30
ALOS-2	Jul 17, 2015 Sep 25, 2015 Jul 15, 2016 Sep 23, 2016	backscattering coefficient (HH, HV)	10	30
Landsat 8	Jul 5, 2015 Sep 7, 2015	band5, band4	30	30
Sentinel-2	Jul 19, 2016 Sep 30. 2016	band8, band4	10	30
Globe-Land30	2010	classes	30	30

April 3, 2014) and Sentinel-1B (launched on April 25, 2016), which shares the same orbital plane, and the repeat cycle at the equator with one satellite is 12 days [41]. It operates in four exclusive acquisition modes: strip map, interferometric wide swath, extrawide swath, and wave mode with different resolutions (down to 5 m) and coverages (up to 400 km). This study used ground range detected high-resolution standard products with vertical–vertical (VV) and vertical–horizontal (VH) polarization in the interferometric wide swath mode (Level 1, https://scihub.copernicus.eu/dhus/#/home). All Sentinel-1 data were preprocessed using the Sentinel Application Platform (SNAP), as follows: updating orbits, thermal noise removal, radiometric calibration, speckle filtering, terrain correction (using the Shuttle Radar Topography Mission digital elevation model at 30 m), and linear to dB conversion. Considering the spatial resolution of other satellite data, the last step is resampled at 30 m. The LIA of Sentinel-1 in Genhe watershed mainly ranges between 20° and 60°. The images collected on July 18 and September 28, 2015, and July 12 and September 22, 2016, were selected for this research during unfrozen seasons (in Table II). Information about the satellite data is shown in Table III.

2) ALOS-2: ALOS-2 is a follow-on mission from the "DAICHI," which was developed by Mitsubishi Electric Corporation under contract to the Japan Aerospace and Exploration Agency (JAXA). ALOS-2 was launched on May 24, 2014, with a revisit time of 14 days. The state-of-the-art Phased Array type L-band Synthetic Aperture

Radar-2 (PALSAR-2) aboard ALOS-2 uses the 1.2 GHz frequency range [42]. ALOS-2 has three main observation modes: spotlight mode (1–3 m), strip map mode (3–10 m), and scan SAR mode (100 m/60 m) [43]. This study used the strip map mode with horizontal–horizontal (HH) and horizontal–vertical (HV) polarizations products (Level 1.5, fine mode, https://satpf.jp/spf/?lang=en). The LIA of ALOS-2 in the Genhe watershed mainly ranges between 10° and 50°. The dates of the selected ALOS-2 images correspond to the Sentinel-1 ones, they are July 17 and September 25, 2015, and July 15 and September 23, 2016 (in Table II), and details of the data are shown in Table III. All of the ALOS-2 data were preprocessed using the ENVI and SNAP Toolboxes, as with Sentinel-1.

C. Optical Data

The free access to both the Sentinel-2 and Landsat 8 data, the similar wavelengths, and the same geographic coordinate system provide an excellent opportunity to use these two types of data [44]. Therefore, we chose Landsat 8 to calculate NDVI for 2015 instead of Sentinel-2 because Sentinel-2 had no released observations from the official website in the Genhe watershed area for 2015. Moreover, Sentinel-2 was used to calculate the NDVI for 2016 due to a large number of clouds present in the Landsat 8 images. If Sentinel-2 and Landsat 8 images that are closest to the SAR images are cloudy, then the optical images were acquired two weeks before or after the SAR acquisitions could be used because the vegetation is assumed to not change significantly within one or two weeks [23]. Details of the data are shown in Table III.

1) Sentinel-2: The Copernicus Sentinel-2 mission comprises a constellation of two polar-orbiting satellites placed in the same Sun-synchronous orbit, namely, Sentinel-2A (launched on June 23, 2015) and Sentinel-2B (launched on March 7, 2017). Each of the satellites in the Sentinel-2 mission hosted a single payload multispectral instrument (MSI) with a ten-day repeat cycle, which covered from the visible and near infrared to the shortwave infrared spectral range [45]. This work used Sentinel-2A MSI data Level 1C (https://scihub.copernicus.eu/dhus/#/home) under cloud-free conditions to calculate the NDVI [(Band8 − Band4)/ (Band8 + Band4), 10 m]. It should be noted that all of the Sentinel-2A data were preprocessed with radiometric correction, atmospheric correction, and resampling at 30 m using the Sentinel-2 Toolbox. Details of the data are shown in Table III.

2) Landsat 8: Landsat 8 was developed in collaboration between the National Aeronautics and Space Administration (NASA) and the U.S. Geological Survey (USGS), and it was launched on February 11, 2013. The satellite carries the Operational Land Imager (OLI) and the TIRS, and it has a 16-day repeat cycle [46]. This work used Landsat 8 OLI/TIRS C1 Level 2 data (https://earthexplorer.usgs.gov/) under cloud-free conditions to calculate NDVI [(Band5 − Band4)/(Band5 + Band4), 30 m]; details of the data are shown in Table III.

D. Land Cover Information

The land cover map used in this article is GlobeLand30-2010 with a 30-m resolution in the baseline year of 2010,

This article has been accepted for inclusion in a future issue of this journal. Content is final as presented, with the exception of pagination.

CUI *et al.*: POTENTIAL OF ALOS-2 AND SENTINEL-1 RADAR DATA FOR SOIL MOISTURE RETRIEVAL 5
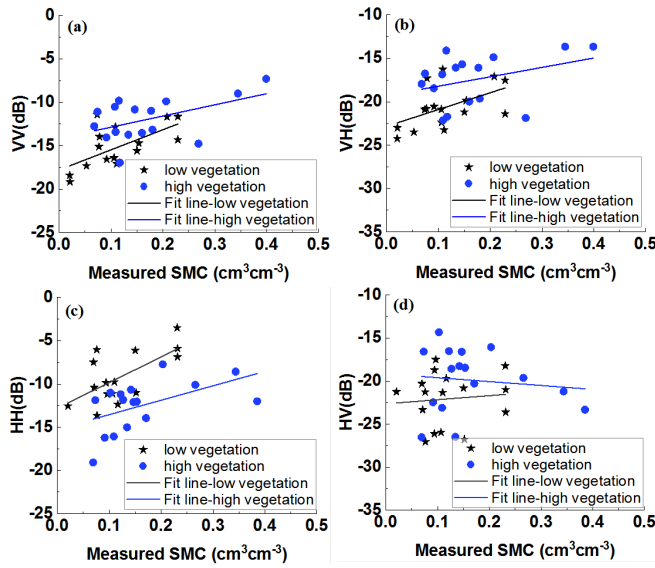

Fig. 2. SAR backscattering coefficient versus measured SMC for low (asterisks) and high (points) vegetated soil. (a) C-band-VV. (b) C-band-VH. (c) L-band-HH. (d) L-band-HV.

TABLE IV
RESULT OF BACKSCATTER COEFFICIENT AND SMC FITTING IN DIFFERENT CONDITIONS

Land surface	Relationship	Linear fit	Logarithm fit
Low Vegetation (grass, shrub, crop)	VV vs. SMC	y=23.16*x-17.80, R^2=0.40	y=2.24 ln(x)-9.84, R^2=0.45
	VH vs. SMC	y=19.32*x-22.84, R^2=0.26	y=1.94 ln(x)-16.03, R^2=0.32
High vegetation (forest)	VV vs. SMC	y=12.88*x-14.16, R^2=0.25	y=2.01 ln(x)-8.16, R^2=0.17
	VH vs. SMC	y=10.82*x-19.30, R^2=0.13	-
Low Vegetation (grass, shrub, crop)	HH vs. SMC	y=29.65*x-12.81, R^2=0.42	y=2.78 ln(x)-2.96, R^2=0.43
	HV vs. SMC	-	-
High vegetation (forest)	HH vs. SMC	y=16.66*x-15.22, R^2=0.27	y=3.58 ln(x)-5.58, R^2=0.36
	HV vs. SMC	-	-

(x=SMC, y= backscatter coefficient with different polarizations and frequencies, R^2 is the square of the correlation coefficient, "-" means that the fitting result is poor and R^2<0.1; VV and VH: Sentinel-1 polarization mode, HH and HV: ALOS-2 polarization mode)

and it was produced by the National Geomatics Center of China (http://www.globallandcover.com/home_en.html?type = data). The GlobeLand30 classification system includes ten land cover types, and the images utilized for classification are multispectral images with a 30-m resolution, including the Landsat TM5 and ETM+, China Environmental Disaster Alleviation Satellite HJ-1, and other auxiliary data [47].

III. DATA ANALYSIS AND METHODS

A. Data Analysis

1) Sensitivity Analysis Between Backscattering Coefficients at C- and L-Bands and SMC: The parameters' sensitivity analysis will help us to select the appropriate configuration that is more sensitive to SMC. This section analyzes the sensitivity of the SAR signal to the SMC in the VV and VH polarizations from Sentinel-1 and in the HH and HV polarizations from ALOS-2, respectively, as shown in Fig. 2 and Table IV. In this study area, the land cover is mainly characterized by crops, grass, shrubs, and forest. Furthermore, the forestland is mainly composed of artificial forest farms, and the percentage of virgin forest is not very high. The observation sites in the forest are mainly located close to the boundary of the forestland and not in the center. According to the vegetation type and vegetation height measurement of sites in the study area, the observation sites were subdivided into two categories of vegetation: low vegetation (crop, grass, and shrub; height approximately ≤2 m) and high vegetation (forest; height approximately >2 m) to better evaluate the sensitivity of the backscattering coefficients in SMC. It should be noted that 2 m is an empirical value applicable to the Genhe study area.

Fig. 2 shows the relationship of the SAR backscattering coefficient at C- (top) and L- (bottom) bands and the measured SMC for low and high-vegetated areas. The backscattering coefficient usually increases with increasing SMC at VV, VH, and HH polarizations [in Fig. 2(a)–(c)]. The SAR signal at

the HV polarization is less sensitive to SMC in the high-vegetation area [in Fig. 2(d)]. The threshold of NDVI is 0.3~0.7 for low vegetation and 0.4~0.85 for high vegetation. As expected, there is a significant decrease in the sensitivity of the radar signals to SMC with the increase in the NDVI. This result is clearly produced by the strong scattering from the high vegetation and the attenuation of soil signals due to high vegetation [15], [23]. A summary of the linear relationships between the backscattering coefficient and SMC at the C- and L-bands in all of the available polarizations is shown In Table IV. The highest sensitivity to SMC is shown at the VV and HH polarizations [in Fig. 2(a) and (c)], and the correlation coefficient R^2 values of logarithm fit are 0.45 and 0.43, respectively, whereas there is a significant decrease in the sensitivity of the VH and HV polarizations to SMC (in Fig. 2(b) and (d) and Table IV). For both of these two frequencies, cross polarization (VH and HV) is less sensitive to SMC than copolarization (VV and HH) due to its high sensitivity to volume scattering, which is caused by the strong scattering contribution of the vegetation [10], [15], [48]. The HV polarization data at the L-band show much lower sensitivity to SMC than VH polarization data at the C-band, which may be related to longer wavelength SAR that is more sensitive to surface roughness than shorter wavelength SAR. The correlation coefficient R^2 values between ALOS-2 HV and roughness, Sentinel-1 VH, and roughness are 0.594 and 0.159, respectively. It means that ALOS-2 HV is more sensitive to surface roughness than the Sentinel-1 VH in the Genhe area. In addition to the influence of frequency on backscattering, the correlation coefficient (R^2) values between ALOS-2 HH and LIA (18°~38°), and Sentinel-1 VV and LIA (34°~48°) are 0.231 and 0.304, respectively. It means

This article has been accepted for inclusion in a future issue of this journal. Content is final as presented, with the exception of pagination.

6   IEEE TRANSACTIONS ON GEOSCIENCE AND REMOTE SENSING
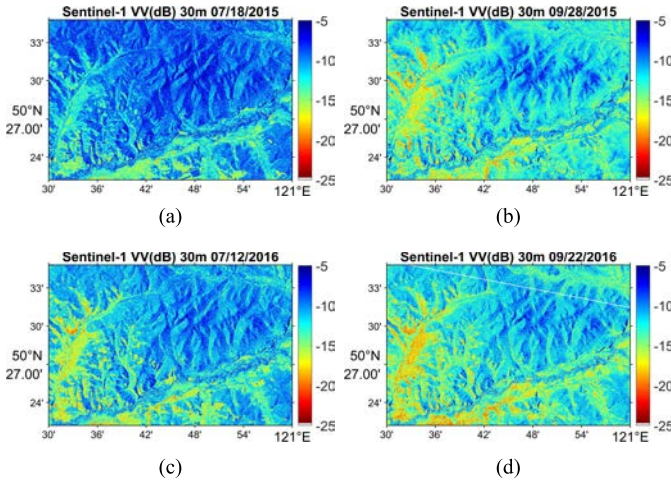

Fig. 3. Spatial distribution of the Sentinel-1 SAR backscattering coefficient for VV on (a) July 18, 2015, (b) September 28, 2015, (c) July 12, 2016, and (d) September 22, 2016.
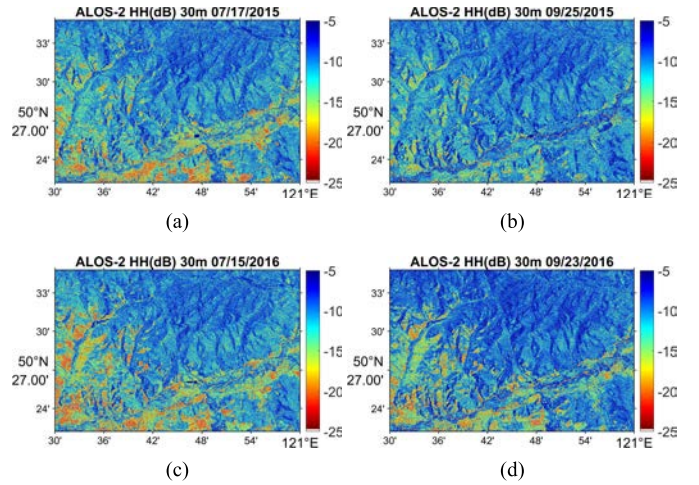

Fig. 4. Spatial distribution of the ALOS-2 SAR backscattering coefficient for HH on (a) July 17, 2015, (b) September 25, 2015, (c) July 15, 2016, and (d) September 23, 2016.

that Sentinel-1 VV is more affected by the LIA than the ALOS-2 HH.

Compared with the result of the linear fit in Table IV, the logarithmic fitting shows higher determination coefficients for Sentinel-1 and ALOS-2, except for the Sentinel-1 VH and VV radar signals in high-vegetated soil. This finding could be due to the influence of the vegetation and surface roughness and to the complex mechanisms between the radar signal and SMC in vegetated soil, which are not simply linear [1].

2) Spatial Pattern of SAR Backscattering Coefficient Characteristics in the Study Area: Based on the above analysis, copolarizations (VV and HH) are demonstrated to be more sensitive to SMC than cross-polarizations (VH and HV). To better understand the copolarization scattering characteristics of Sentinel-1 and ALOS-2, this section presents the spatial distribution of Sentinel-1 SAR backscatter-VV and ALOS-2 SAR backscatter-HH at a 30-m resolution, as shown in Figs. 3 and 4.

Fig. 3 shows the spatial distribution of the SAR backscatter-VV from Sentinel-1, and it is apparent that the backscatter-VV in July [see Fig. 3(a) and (c)] is mostly higher than that in September [see Fig. 3(b) and (d)]. This because July is the thickest time of the year for vegetation, and NDVI is approximately at its maximum, with 0.85 in a high-vegetation area over the Genhe watershed. Moreover, the backscattering coefficient increases due to the increase in the direct scattering from the upper canopy [49]. Vegetation began to wither in September (NDVI < 0.7), and the backscattering coefficient decreased due to the decrease in the canopy attenuation [50]. Corresponding to the land classification map (see Fig. 1), the backscatter-VV in the high-vegetation area is higher than that in the low-vegetation area. Compared with other land cover types, the backscatter of cultivated land is the lowest. This finding could be related to the scattering mechanism of canopy types.

In Fig. 4, the distribution of backscatter-HH from ALOS-2 SAR is consistent with Sentinel-1 backscatter-VV, and the ALOS-2 backscatter-HH in low-vegetation areas is lower than that in the high-vegetation areas (NDVI approximately
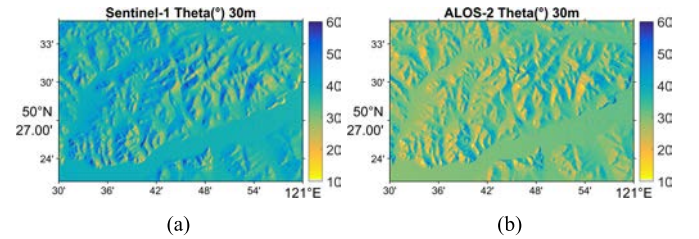

Fig. 5. Spatial distribution of the SAR LIA in Genhe area. (a) Sentinel-1 LIA. (b) ALOS-2 LIA.

0.85). The backscatter of cultivated land is lower than that of other land covers (grass and forest). The spatial distribution of backscatter-HH in high-vegetation areas is similar on July 18 and September 28, 2015 [see Fig. 4(a) and (b)] and July 12 and September 22, 2016 [see Fig. 4(c) and (d)]. The ALOS-2 SAR backscattering coefficient seems higher in September than in July, which could be due to the strong penetration capacity of the L-band [51], and it is less affected by the scattering of the canopy. Moreover, SMC measurements are wetter in September than in July [3].

The spatial distribution of the Sentinel-1 SAR incidence angle and ALOS-2 SAR incidence angle is shown in Fig. 5. The incidence angles of Sentinel-1 and ALOS-2 are mainly between 20° and 60° [see Fig. 5(a)] and 10° and 50° [see Fig. 5(b)], respectively. Corresponding to the land classification map (see Fig. 1), the incidence angle of Sentinel-1 is approximately 10° higher than that of ALOS-2 in grassland, shrubland, cropland, and forestland. From the comparison of the spatial distribution of Sentinel-1 backscatter-VV with the ALOS-2 backscatter-HH, the ALOS-2 backscatter is higher than Sentinel-1 backscatter in the high-vegetation areas, especially on September 23, 2016 [see Figs. 3(d) and 4(d)]. This because the ALOS-2 incidence angle is usually lower than the Sentinel-1 incidence angle [see Fig. 5(a) and (b)] and that the backscattering coefficient decreases with increasing incidence angle [52]. Moreover, the HH backscatter is higher than the VV backscatter at incidence angles of >20°, and the HH backscatter is lower than the VV backscatter at incidence angles of <20° in vegetated soil [52], [53].
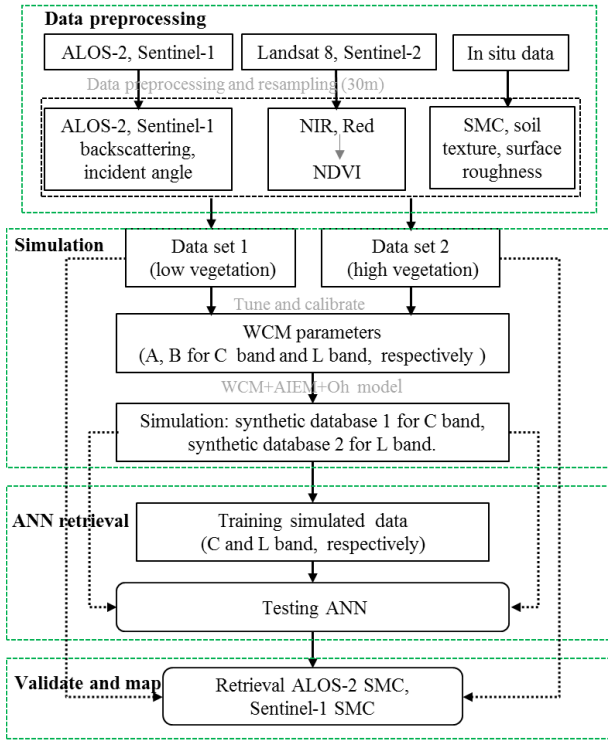
This article has been accepted for inclusion in a future issue of this journal. Content is final as presented, with the exception of pagination.

CUI *et al.*: POTENTIAL OF ALOS-2 AND SENTINEL-1 RADAR DATA FOR SOIL MOISTURE RETRIEVAL

7

Fig. 6. Flowchart of the SMC retrieval methodology.

B. Methods

The influence of vegetation, surface roughness, and the complex mechanisms that regulate radar signals and SMC in vegetated soil is not simple to describe [1], [22]. ANN methods provide an alternative to traditional numerical modeling techniques [54] because they can describe the complex relationships between the input and output parameters. During the prediction phase, if a sufficiently robust and representative set of samples were provided during the training phase, the ANN would significantly reduce the computational time [55] and would be able to estimate and map the SMC from Sentinel-1 and ALOS-2 SAR data with reasonable accuracy. The training set used in the ANN derives from a synthetic database for the C-band and L-band obtained through the calibrated WCM combined with the AIEM and the Oh model. The flowchart of the SMC retrieval method is shown in Fig. 6.

1) Land Surface Synthetic Database Based on Electromagnetic Model Simulations: WCM was developed first by Attema and Ulaby [20] in 1978. In the WCM, the total backscatter (σ_{pq}^0) is expressed as the incoherent sum of direct backscattering of the vegetation layer (σ_{pq_Veg}) and backscatter from the underlying surface $(\sigma_{pq\_Soil}^0)$, which is attenuated by the vegetation layer through the two-way attenuation factor (τ^2), and multiple scattering in soil vegetation is generally neglected. The original model was subsequently modified or extended by various authors [25], [56]–[58]. In this work, WCM was simplified to [58]

$$\sigma_{pq}^0 = \sigma_{pq\_Veg}^0 + \tau^2 \cdot \sigma_{pq\_soil}^0 \quad (1)$$

$$\sigma_{pq\_Veg}^0 = A \cdot V_{eg} \cdot \cos\theta(1 - \tau^2) \quad (2)$$

$$\tau^2 = \exp(-2 \times B \cdot V_{eg} \cdot \mathrm{Sec}\theta) \quad (3)$$

TABLE V
FITTING AND VALIDATION OF THE *A* AND *B* PARAMETERS IN THE WCM FOR EACH POLARIZATION USING SATELLITE DATA AND *IN SITU* DATA

Band	Land cover	Pol	A	B	R	RMSE (dB)	Bias (dB)
C band	Low vegetation	VV	0.004	0.125	0.97	0.87	0.40
		VH	0.387	0.055	0.89	1.61	0.60
	High vegetation	VV	0.250	0.155	0.94	0.88	0.07
		VH	0.086	0.020	0.69	1.76	0.05
L band	Low vegetation	HH	0.145	0.204	0.96	0.74	0.07
		HV	0.278	0.023	0.72	2.34	-0.17
	High vegetation	HH	0.061	0.065	0.95	1.10	0.37
		HV	0.213	0.024	0.91	2.34	1.80

(Pol: Polarization mode, R is the correlation coefficient, RMSE is the root mean square error, Bias is the mean bias)

where pq is polarization. θ is the incidence angle. Parameters *A* and *B* are parameters that depend on the canopy descriptors and radar configurations. Veg is the vegetation's descriptor (such as vegetation water content (VWC), Leaf Area Index (LAI), and NDVI). In this work, NDVI was used as a vegetation parameter in WCM because it can be easily derived from optical images with a resolution of 30 m.

Some studies have shown that WCM, AIEM, and Oh models have high potentials for soil moisture retrieval [22], [58]–[60]. Therefore, WCM, AIEM (HH and VV) [18], and Oh (VH or HV) [61] were used in this work. In the WCM, the radar backscatter of the bare soil was simulated by the AIEM (HH and VV) and Oh models (VH or HV) at the C-band and L-band. Parameters *A* and *B* are estimated empirically by fitting the ground observations and models with the Nelder–Mead minimization method [62]. To better characterize the backscattering in the presence of different land cover, the vegetation surface is subdivided into low-vegetation surfaces (grass, crop, and shrub) and high-vegetation (forest) surfaces. In Table V, the fitting and validation of the *A* and *B* parameters in the WCM are shown for the C-band (VV, VH) and L-band (HH and HV) with the different vegetation covers. The validation of the parameters between the calibrated model and the observed data shows that the accuracy of the copolarization (VV and HH) is better than for the cross-polarization (VH and HV), and the fitting result in the presence of low vegetation is better than in the high-vegetation areas. Moreover, some studies have shown that copolarization (VV and HH) provides higher accuracy on the SMC retrieval than cross-polarization (HV and VH) [22], [23]. Based on these findings, the considered SMC retrieval configuration is limited to VV and HH polarization.

With the *A* and *B* parameters (see Table V), the land surface synthetic databases are built by the WCM combined with AIEM and the Oh model for the C- and L-bands, respectively. The input parameters for the C- and L-bands have the same ranges of values, and the details of input parameters are given as follows: 1) SMC, random between 0.02 and 0.42 cm³/cm³; 2) incidence angle, random between 10° and 60°; 3) root mean square height *s*, random between 0.6 and 6 cm; 4) correlation length *l*, random between 2 and 20 cm, $0 < s/l < 0.4$; the exponential autocorrelation function was used in this work; and 5) NDVI, random between 0 and 0.85.
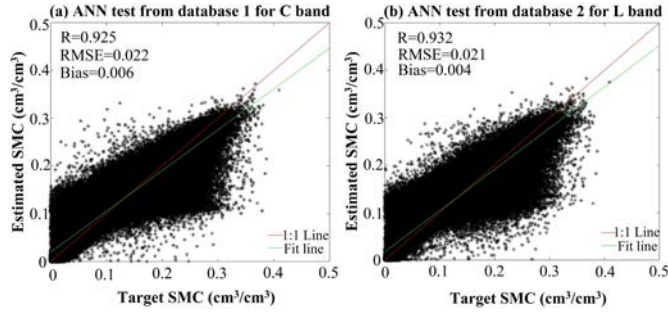
This article has been accepted for inclusion in a future issue of this journal. Content is final as presented, with the exception of pagination.

8 IEEE TRANSACTIONS ON GEOSCIENCE AND REMOTE SENSING

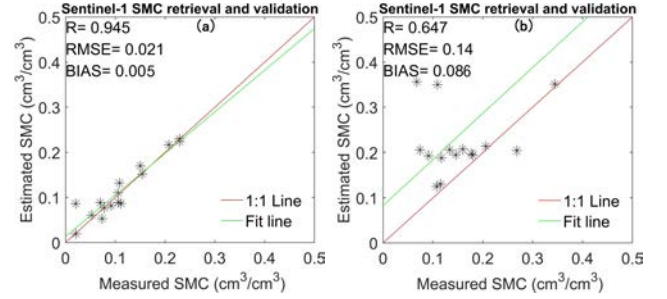Fig. 7. Training results of the ANN test from (a) database 1 for C-band and (b) database 2 for L-band.

Fig. 8. Validation of the Sentinel-1SMC retrieval. (a) Low vegetation. (b) High vegetation.

Fig. 9. Validation of the ALOS-2 SMC retrieval. (a) Low vegetation. (b) High vegetation.

2) ANN Algorithm: The SMC retrieval algorithm is based on the feedforward multilayer perceptron ANN proposed in [22], which consists of number of hidden layers of neurons between the input and the output. The training of the ANN follows the backpropagation learning rule, which can minimize the error between the desired target parameters and the actual output parameters. At the same time, to obtain the optimal ANN architecture with the terms for the neurons and hidden layers, the ANN configuration often starts with a simple combination of hidden layers and neurons, and there is an addition of neurons and hidden layers to increase the ANN configuration. There is repeated training and testing with error comparisons, until the optimal ANN configuration is found to have a negligible error between the training and testing sets.

According to the above model simulation, the land surface synthetic database was composed of parameters that include the backscattering coefficient, the incidence angle, SMC, roughness, and vegetation parameters for the C-band (database 1) and L-band (database 2), respectively. In this work, an optimal ANN architecture with two hidden layers of eight neurons was selected for matching the C-band and L-band data. In the ANN training, database 1 and database 2 are randomly sampled into two subsets: 50% of the data were selected as the training data and 50% of the data were used to test the training results. In accordance with the acquisition modes of Sentinel-1, the input parameters of the ANN are the VV backscattering coefficient, the incidence angle, and NDVI from database 1, and the output parameter is the SMC. In accordance with the acquisition modes of ALOS-2, the input parameters of the ANN are the HH backscattering coefficient, the incidence angle, and NDVI from database 2, and the output parameter is the SMC.

The training results of the ANN test for C-band database 1 and L-band database 2 are shown in Fig. 7. In the test, the number of each parameter in database 1 and database 2 is 2 000 000. Here, 50% of the data are randomly selected as training data, and the remaining 50% of the data are used to test the training results. Therefore, database 1 and database 2 are subjected to random sampling in two subsets, each of size 1 000 000. In Fig. 7, the target SMC is derived from C-band database 1 and L-band database 2, and the estimated SMC is retrieved by the ANN. The estimated SMC and target SMC have a significant correlation. R and root mean square error (RMSE) of database 1 are 0.925 and 0.022 cm^3/cm^3 (see Fig. 7(a) for database 1); R and RMSE of database 2 are 0.932 and 0.021 cm^3/cm^3 (see Fig. 7(b) for database 2), respectively. The test results show that the ANN's training settings are reliable, and they can be used for subsequent SMC retrieval.
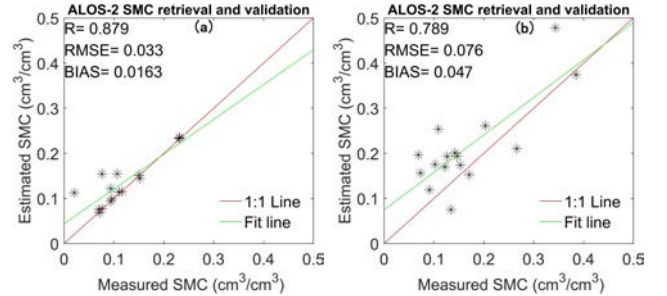
IV. RESULTS AND DISCUSSION

A. SMC Retrieval Validation Using Ground Site Data

Based on the above ANN algorithm, the SMC is estimated from the Sentinel-1 and ALOS-2 SAR data. The results of the SMC retrievals from the Sentinel-1 and ALOS-2 SAR data are compared with the *in situ* SMC for low- and high-vegetation areas, respectively, as shown in Figs. 8 and 9.

Sentinel-1 and ALOS-2 SMC retrievals had the highest accuracy for the low-vegetation covered areas (crop, grass, and shrub), with R of 0.945 and 0.879 and RMSE of 0.021 and 0.033 cm^3/cm^3 [see Figs. 8(a) and 9(a)], respectively. However, with the soil covered with high vegetation (forest), the ALOS-2 SMC retrievals provide, as expected, higher accuracy (with R of 0.79 and RMSE of 0.076 cm^3/cm^3) than the Sentinel-1 SMC retrievals ($R = 0.65$ and RMSE $= 0.14$ cm^3/cm^3) in Figs. 8(b) and 9(b), respectively. This finding is due to the strong attenuation of the SAR signal by high vegetation when the NDVI value was greater than 0.7 [48]. Moreover, Section III showed that the sensitivity of the C- and L-band SAR signals to SMC for NDVI 0.3∼0.7 (low vegetation) is higher than that for an NDVI 0.4∼0.85 (high vegetation).

By comparing Sentinel-1 and ALOS-2 SMC retrievals, we can note that the accuracy of the Sentinel-1 retrievals is higher than the accuracy of the ALOS-2 retrievals in low-vegetation areas. For low-vegetation areas, the high sensitivity was obtained from VV polarization of Sentinel-1 ($R^2 = 0.45$) and HH polarization of ALOS-2 ($R^2 = 0.43$) in Table IV. The

This article has been accepted for inclusion in a future issue of this journal. Content is final as presented, with the exception of pagination.

CUI *et al.*: POTENTIAL OF ALOS-2 AND SENTINEL-1 RADAR DATA FOR SOIL MOISTURE RETRIEVAL   9

results demonstrated that the potential of Sentinel-1 for SMC estimation was higher than ALOS-2 over low-vegetation areas. This finding corresponds to the results of recent studies [48], [63] showing that the SMC estimates from the L-band generally exhibited RMSE values greater than those obtained for the C-band in wheat, grassland, and bare soil. For the case without vegetation or with low-vegetation cover, the contribution of low-vegetation areas to the total scattering is negligible at L-band and C-band. The C-band SAR is more sensitive to soil moisture and less sensitive to surface roughness than L-band SAR [64], [65], which is one of the reasons that the accuracy of the Sentinel-1 retrievals is higher than the accuracy of the ALOS-2 retrievals in low-vegetation areas. With the soil covered with high vegetation, the RMSE of Sentinel-1 SMC retrievals is 0.064 cm^3/cm^3 higher than ALOS-2 SMC retrievals. This finding is due to the higher frequency (C-band), which is less able to penetrate the densely vegetated surfaces with respect to the longer wavelength L-band and the negligible SMC contribution at the C-band [51].

Overall, VV polarization monitors early canopy growth best, while HH polarization is better during the later stages of canopy development [59], [66]. Moreover, the canopy loss and the volume scattering coefficient increase with the frequency [67] and will decrease the sensitivity of the C-band to SMC compared with the L-band. The accuracy of the ALOS-2 and Sentinel-1 SMC retrievals is higher in low-vegetation areas than in high-vegetation areas. These results show that both the C-band and L-band can satisfy the accuracy of the SMC retrieval in low-vegetation areas. The L-band HH polarization presented better accuracy results than the C-band VV polarization in high-vegetation soils.

B. Influence of Local Incidence Angle on SMC Retrievals

The sensitivity of the backscattering coefficient at L-HH and C-VV decreases with increasing incidence angle [68]. The incidence angles of Sentinel-1 and ALOS-2 are mainly 20°~60° and 10°~50°, respectively. The radar incidence angle has a large range of variation, and it is difficult to normalize to a fixed angle due to the unavoidable influence of the incidence angle on the retrieval of soil moisture. This is the reason for accounting for the incidence angle as an input parameter in this work since it is a factor that affects the SMC retrieval. Therefore, the influence of incidence angle on the accuracy of SMC retrievals is discussed in this part.

Based on the *in situ* measurements and SAR data, the accuracy of SMC retrievals at different incidence angles was calculated, as shown in Table VI. Corresponding to the *in situ* measurements, the incidence angles of Sentinel-1 are mainly 35°~56°, and the incidence angles of ALOS-2 are mainly 20°~37°. Sentinel-1 SMC retrievals have higher RMSE at 35°, 37°, and 38°, which are 0.17, 0.053, and 0.071 cm^3/cm^3, respectively. ALOS-2 SMC retrievals have higher RMSE at 30°, 32°, and 37°, which are 0.087, 0.067, and 0.058 cm^3/cm^3, respectively. Coincidentally, these SMC retrievals with higher errors are mainly in forest areas. Moreover, the number of samples is too small at different incidence angles, and it is difficult to find out whether the main influence factor is the LIA or the surface roughness or vegetation.

TABLE VI
ERROR METRICS FOR SENTINEL-1 AND ALOS-2 SMC
RETRIEVAL AT DIFFERENT LIAS

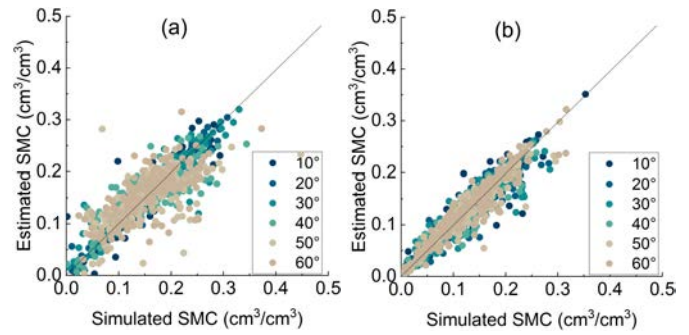| SAR	LIA (°)	R	RMSE (cm^3/cm^3)	Bias (cm^3/cm^3)	No.
Sentinel-1	35	0.670	0.170	0.126	4
	37	0.840	0.053	0.024	8
	38	0.879	0.071	0.054	8
	43	0.921	0.013	0.003	4
	46	0.964	0.012	0.001	4
	56	0.864	0.016	0.004	4
ALOS-2	20	0.933	0.028	0.012	8
	24	0.750	0.024	0.011	4
	30	0.816	0.087	0.046	8
	31	0.745	0.012	0.010	4
	32	0.822	0.067	0.038	4
	37	0.962	0.058	0.057	4

(No. is the number of samples)

Fig. 10.   Validation of SMC estimates from (a) C-band and (b) L-band simulated database at different LIAs.

TABLE VII
ERROR METRICS FOR C- AND L-BAND SMC ESTIMATES
AT DIFFERENT LIAS

SAR	LIA (°)	R	RMSE (cm^3/cm^3)	Bias (cm^3/cm^3)	No.
C-band	10	0.666	0.047	-0.008	200
	20	0.942	0.022	0.003	200
	30	0.985	0.011	0.009	200
	40	0.932	0.022	0.006	200
	50	0.882	0.034	0.002	200
	60	0.713	0.040	0.002	200
L-band	10	0.765	0.028	0.004	200
	20	0.918	0.020	-0.002	200
	30	0.940	0.019	-0.01	200
	40	0.953	0.017	0.001	200
	50	0.852	0.019	0.001	200
	60	0.783	0.032	0.001	200

The land surface synthetic database has sufficient samples, therefore, 200 samples were randomly selected at 10°, 20°, 30°, 40°, 50°, and 60° in the C-band and L-band simulated databases to retrieve and validate SMC and analyze the effect of incidence angle on the accuracy of SMC retrievals. The results of the SMC retrievals from the C-band and L-band simulated database are compared with the simulated SMC at different incidence angles, as shown in Fig. 10 and Table VII.

From Fig.10 and Table VII, we can see that C- band and L-band SMC retrievals have higher RMSE at low incidence angle (<20°) and high incidence angle (>50°). SAR at a low

This article has been accepted for inclusion in a future issue of this journal. Content is final as presented, with the exception of pagination.

10

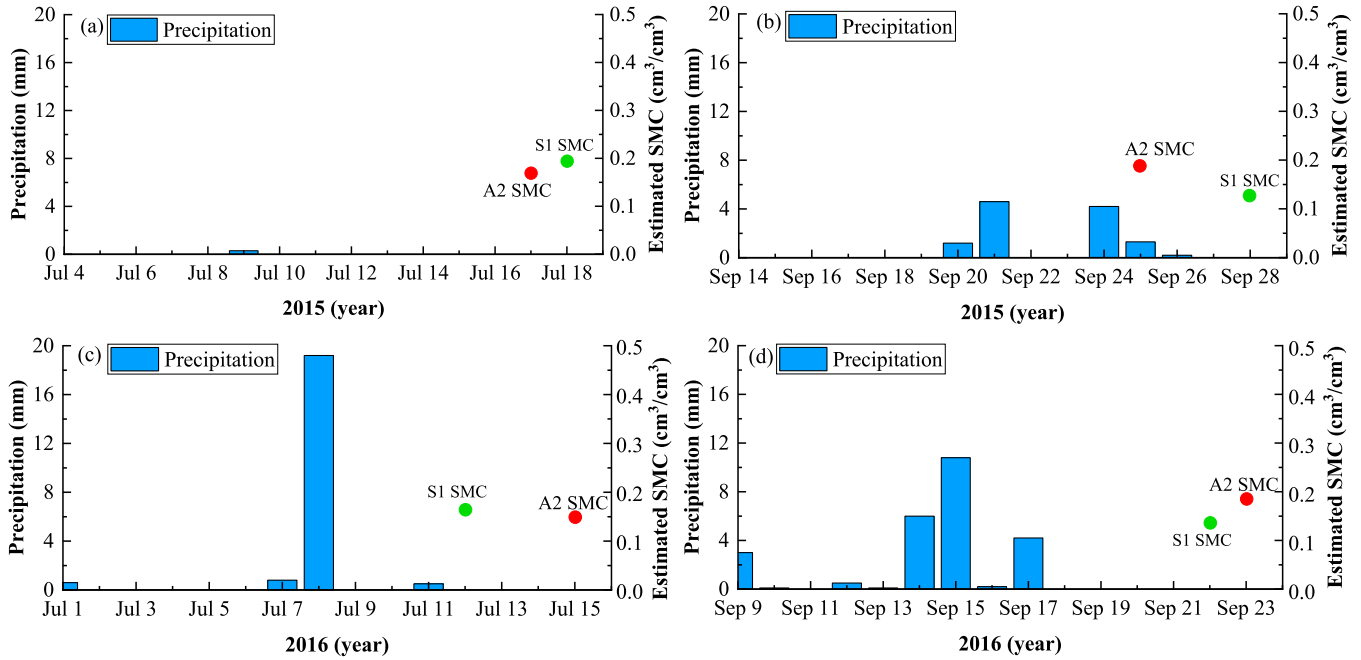IEEE TRANSACTIONS ON GEOSCIENCE AND REMOTE SENSING

Fig. 11. Daily precipitation in the Genhe watershed area (A2 SMC-red circle: ALOS-2 SMC; S1 SMC-green circle: Sentinel-1 SMC). (a) July 4–18, 2015. (b) September 14–28, 2015. (c) July 1–15, 2016. (d) September 9–23, 2016.

angle of incidence has a shorter path length within vegetation volume, and hence, the SAR signal at a low incidence angle is able to penetrate up to the soil underneath. Therefore, the low incidence angle SAR backscatter is affected by the soil surface contribution (SMC and roughness) even in vegetated areas [69]. Meanwhile, backscattering coefficients are more sensitive to roughness conditions at the L-band compared to the C-band [70]. However, the penetration depth could generate some differences and limitations in methodologies; the influence of moisture profile heterogeneities at the L-band is less than that of the C-band because the L-band penetration depth is approximately 5 cm for medium moisture levels [71]. Therefore, the accuracy of L-band soil moisture is higher than that of the C-band. Moreover, some studies have indicated that a higher incidence angle increases the path length of the SAR signal through the vegetation volume, resulting in higher interaction with crop canopy [72]. The SAR signal at a high incidence angle is more sensitive to surface roughness and vegetation than at a low incidence angle [64], [73]. This is the reason that the accuracy of SMC retrievals is not high at a large incidence angle. The influence of incidence angle is considered in the algorithm. Meanwhile, some studies have indicated that the incidence angles from 30° to 50° do not have a significant impact on the sensitivity of HH and VV to the variation of SMC [1], and the errors of the SMC estimates do not significantly depend on the incidence angles (20°∼45°) [23]. In this work, the incidence angle (20°∼50°) has little effect on the accuracy of SMC retrievals, and the accuracy of the C-band soil moisture at 30° and the L-band soil moisture at 40° is higher than that of other incidence angles. The precondition of the conclusion in the work is that the influence of incidence angle has been considered in the soil moisture retrieval algorithm.

C. Response of SMC Retrievals to Rainfall

Generally, the occurrence of rainfall will increase the SMC suddenly [74]. To examine the reasonableness of SMC retrievals further, the daily rainfall data from the China Meteorological Data Service Center (0.5° × 0.5°, http://data.cma.cn/data/cdcdetail/dataCode/SURF_CLI_CHN_PRE_DAY_GRID_0.5.html) were used to investigate the response of SMC retrieval to rainfall in this part. Corresponding to the local overpass time of the satellite, two weeks of daily rainfall are displayed in Fig. 11, the red circle represents the ALOS-2 mean SMC estimation during its overpass in the study area, and the green circle represents the Sentinel-1 mean SMC estimation during its overpass in the study area.

There are no significant rainfall events, and the cumulative rainfall is less than 10 mm in one week before the Sentinel- and ALOS-2 satellite overpass during the period of July 11–18, 2015 [see Fig. 11(a)] and September 16–23, 2016 [see Fig. 11(d)]. Therefore, the influence of rainfall on the SMC retrieval can be ignored during the period July 11–18, 2015 [see Fig. 11(a)] and September 16–23, 2016 [see Fig. 11(d)]. During September 21–28, 2015 [see Fig. 11(b)], the cumulative rainfall is 10.3 mm, and there are slight rainfall events on September 24 and 25, 2015 (4.2 mm, 1.3 mm), which is very close to the ALOS-2 overpass. However, there are no rainfall events on September 27 and 28, 2015, which is close to the Sentinel-1 overpass. Meanwhile, the ALOS-2 SMC on September 25, 2015, is higher than the Sentinel-1 SMC on September 28, 2018. The results indicate that, when the rainfall (<10 mm) arrives one or two days before the ALOS-2 overpass time, the ALOS-2 SMC can capture the influence of rainfall on soil moisture. During July 5–15, 2016 [see Fig. 11(c)], the cumulative rainfall is

19.7 mm, and there are the moderate rainfall (19.2 mm) events on July 8, 2015, four days before the Sentinel-1 overpass, and the slight rainfall (0.5 mm) events on July 11, 2015, one day before the Sentinel-1 overpass. Moreover, the Sentinel-1 SMC July 12, 2015, is higher than ALOS-2 SMC July 15, 2015. The results show that, when the rainfall (19.7 mm) arrives four days before the Sentinel-1 overpass time, the Sentinel-1 SMC also can capture the influence of rainfall on soil moisture. Therefore, the Sentinel-1 and ALOS-2 SMC have a good response to rainfall events. There are no rainfall events, and the Sentinel-1 SMC is 0.035 cm^3/cm^3 higher than the ALOS-2 SMC on July 17, 2015, in Fig. 11(a), while the ALOS-2 SMC is 0.049 cm^3/cm^3 higher than the Sentinel-1 SMC on September 23, 2016, in Fig.11 (d). These are because the Sentinel-1 VV-backscattering coefficient is 1.427 dB higher than the ALOS-2 HH backscattering coefficient on July 17, 2015 [in Figs. 3(a) and 4(a)], and ALOS-2 HH backscattering coefficient is 2.168 dB higher than Sentinel-1 VV-backscattering coefficient on September 23, 2016 [see Fig. 3(d) and 4(d)].

Overall, when the rainfall is relatively light (<10 mm), the surface evapotranspiration and vegetation interception make it difficult to store water on the land surface [76], [77], and this fact could have an instantaneous effect on the surface SMC, for example, September 2015 [see Fig. 11(b)]. However, this aspect has a small effect on the SMC after a few days, and the effects can be neglected, such as July 2015 and September 2016 [see Fig. 11(a) and (d)]. When the rainfall intensity increases, the moderate rain (∼19.2 mm) could have a potential impact on the surface SMC due to the infiltration of the rainfall, which could have an effect on the surface SMC in the next few days [75], especially during July 2016 [see Fig. 11(d)]. Therefore, in this work, with the cumulative rainfall being less than 10 mm in one week or five days before the satellite pass, the effect of light rainfall (<10 mm) on SMC can be ignored. If the light rainfall (<10 mm) arrives one or two days before the satellite pass, it surely has some effects on the soil moisture. If the moderate rainfall (≥10 mm) arrives four days before the satellite pass, it has a significant effect on the SMC. Overall, Sentinel-1 and ALOS-2 SMC retrievals have a good response to rainfall events.

D. SMC Mapping

Based on the ANN method, Sentinel-1 SMC maps with a 30-m spatial resolution have been generated on July 18 and September 28, 2015, and on July 12 and September 22, 2016, and they are shown in Fig. 12. ALOS-2 SMC maps with a 30-m spatial resolution obtained on July 17 and September 25, 2015, and on July 15 and September 23, 2016, are shown in Fig. 13. Considering the information on the land cover, the SMC could not be retrieved under the water bodies and the artificial surfaces with the input of land cover information from GlobeLand30-2010.

According to the spatial distribution of the Sentinel-1 SMC and the land classification map (in Figs. 1 and 12), it can be seen that the Sentinel-1 SMC is mostly higher in July than in September, except for some high-vegetation areas. The Sentinel-1 SMC retrievals on July 18, 2015, are higher than the SMC retrievals on July 12, 2016. Corresponding to the
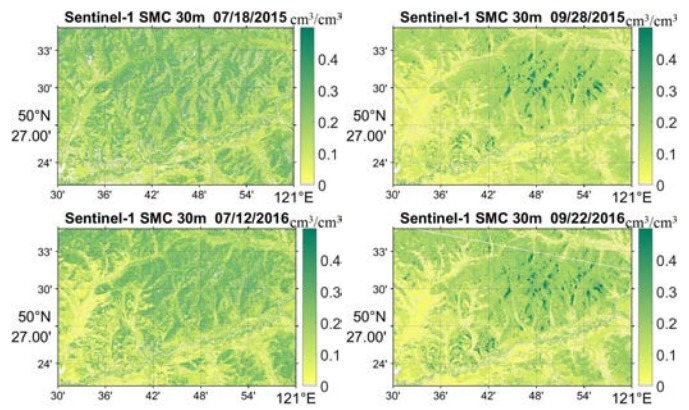
Fig. 12. Spatial distribution of Sentinel-1 SMC retrieval.
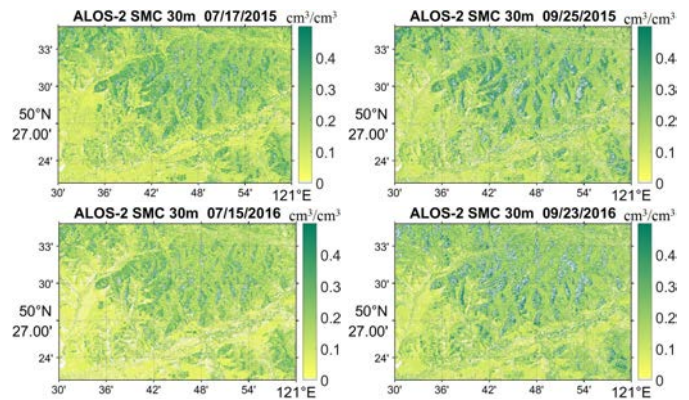
Fig. 13. Spatial distribution of ALOS-2 SMC retrieval.

land classification map (see Fig. 1), the SMC in the high-vegetation area is higher than that in the low-vegetation area, due to the presence of high vegetation, which can reduce the evaporation and maintain higher levels of water content [78]. ALOS-2 SMC maps on July 17 and September 25, 2015, and on July 15 and September 23, 2016, are shown in Fig. 13. The spatial distribution of the soil wet and dry conditions is consistent with the Sentinel-1 retrievals, and the ALOS-2 SMC is lower in low-vegetation areas than in high-vegetation areas. The ALOS-2 SMC retrievals in September are higher than the SMC retrievals in July. In addition, the ALOS-2 and Sentinel-1 SMC retrievals show many missing values in the high-vegetation area due to the decreasing sensitivity to SMC as the canopy height and NDVI increase (approximately 0.85), except for the water bodies and artificial surfaces.

The spatial distribution of SMC retrieval is correlated with the SAR backscattering coefficient, and the backscatter coefficient increases with the SMC (in Figs. 3 and 12 for Sentinel-1 and Figs. 4 and 13 for ALOS-2). Sentinel-1 backscatter is lower than ALOS-2 backscatter on September 28, 2015, and September 22, 2016. This is the reason that the ALOS-2 SMC retrievals on September 25, 2015, and September 23, 2016, are higher than the Sentinel-1 SMC retrievals on September 28, 2015, and September 22, 2016. Meanwhile, Sentinel-1 backscatter is higher than ALOS-2 backscatter on July 18, 2015. This is the reason that the Sentinel-1 SMC retrievals on July 18, 2015, are higher than the SMC retrievals on July 18, 2015. This finding corresponds to that the backscat-

This article has been accepted for inclusion in a future issue of this journal. Content is final as presented, with the exception of pagination.

12   IEEE TRANSACTIONS ON GEOSCIENCE AND REMOTE SENSING
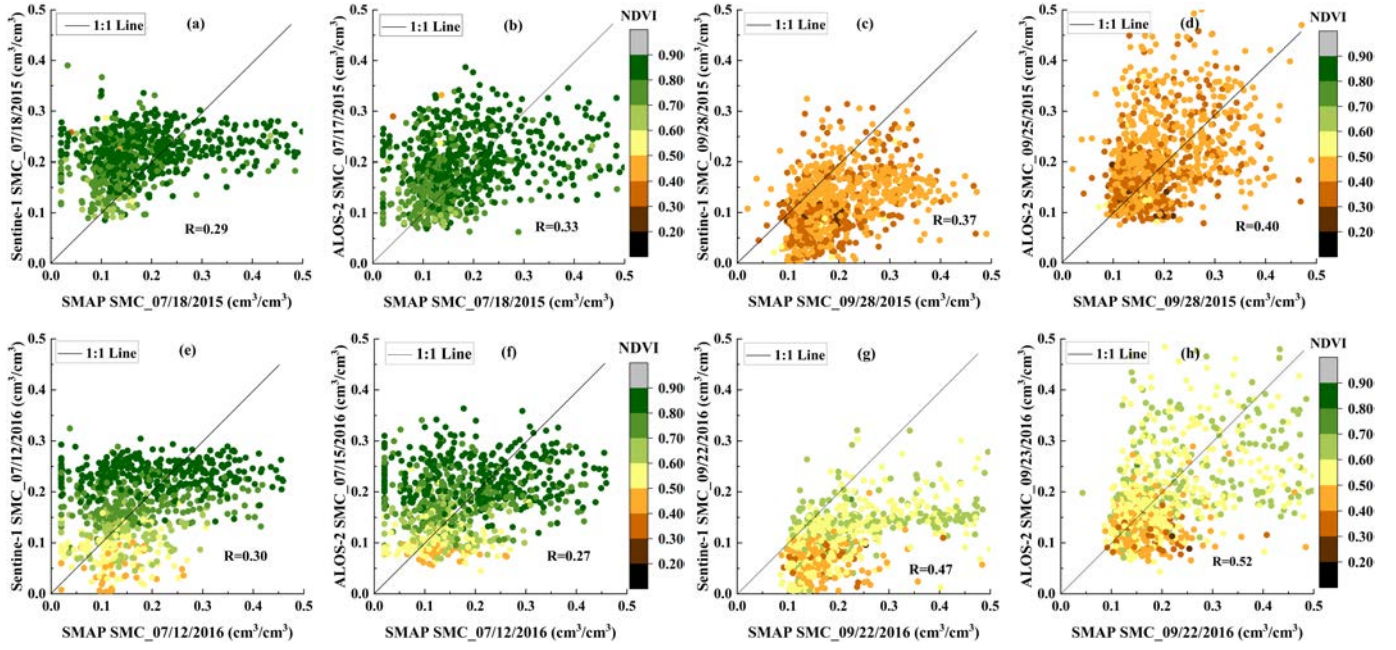
Fig. 14.   1-km resolution aggregated ALOS-2 and Sentinel-1 SMC versus SMAP SMC. (a), (c), (e), and (g) Sentinel-1 versus SMAP. (b), (d), (f), and (h) ALOS-2 versus SMAP.

tering coefficient usually increases with increasing SMC at VV and HH polarizations [63]. Although the SAR images have been processed by speckle filter, the speckle noise still appeared in Sentinel-1 and ALOS-2 soil moisture maps at high-vegetation areas. Some studies have shown that upscaling the SAR signal or using an effective speckle filter operator can reduce the speckle noise [14], [79], which is helpful for soil moisture retrieval at high spatial resolution by SAR.

The C-band backscatter SAR signal is less sensitive to SMC under dense and high-vegetation covers and high incidence angle (NDVI > 0.7 and LIA > 50°), and SAR data are more sensitive to soil roughness at high incidence angles [73]. Consequently, the SMC retrievals become unreliable. On the other hand, the accuracy of ALOS-2 in SMC retrievals is higher than the accuracy provided by Sentinel-1 in the high-vegetation area (see Section IV-A). Because L-band observations correspond to a deeper layer of the land surface compared to C-band [48], [63], however, ALOS-2 SMC retrievals have higher RMSE at low incidence angle (LIA < 20°) in the high-vegetation area (refer to Fig. 5 and Section IV-B).

E. SMC Map Validation Using the SMAP
L2 Radiometer/Radar SMC Product

The validation of SMC retrievals is limited by the lack of ground observations. Previous studies have shown that the accuracy of SMAP SMC is higher than AMSR2 and SMOS SMC in the Genhe watershed area [3]. Moreover, the SMAP and Sentinel-1 SMC product (SMAP L2_SM_SP) have a high resolution of 1 km/3 km, which combines the advantages of L-band radiometer measurements and of C-band radar measurements [80]. Therefore, in order to understand and analyze the reasonability of the spatial distribution of SMC retrievals at high resolution from SAR, we selected

the currently published SMC product with a high spatial resolution (1 km), namely, SMAP L2 active and passive SMC products (https://nsidc.org/data/SPL2SMAP_S/versions/3) as SMC reference data to intercompare the spatial distribution of the ALOS-2 and Sentinel-1 SMC. The SMAP L2 active and passive SMC algorithm is based on disaggregated brightness temperatures and ancillary data using a single-channel algorithm to retrieve the SMC. The disaggregated brightness temperature of the SMAP L-band radiometer is obtained by using the finer spatial resolution of the Sentinel C-band SAR data and parameters derived from a relationship between the brightness temperature and the SAR data [80].

The SMAP L2 radiometer/radar SMC product was validated by the *in situ* measurements before use in this work. The results show that SMAP can represent surface soil moisture to some extent. R and bias between SMAP SMC and *in situ* measurements are 0.649 and 0.035 cm^3/cm^3, respectively. The RMSE of SMAP L2 SMC product is 0.075 cm^3/cm^3 in the Genhe area. It should be noted that the validation of SMAP L2 SMC retrievals is limited by the lack of ground observations. This part mainly analyzes the reliability of the spatial distribution of soil moisture. To facilitate intercomparison, the spatial resolutions of the ALOS-2 and Sentinel-1 SMC are aggregated from 30 m to 1 km. The overpass time of Sentinel-1 is closer to SMAP L2 than that of ALOS-2. Therefore, the comparison between ALOS-2 and SMAP can only be used as a reference analysis due to the difference in the overpass times.

The results of the ALOS-2 and Sentinel-1 SMC estimation versus the SMAP SMC are shown in Fig. 14 and Table VIII. As shown in Table VIII, the correlation between Sentinel-1 SMC, ALOS-2 SMC, and SMAP is higher in September [see Fig. 14(c), (d), (g), and (h)] than in July [see

This article has been accepted for inclusion in a future issue of this journal. Content is final as presented, with the exception of pagination.

CUI *et al.*: POTENTIAL OF ALOS-2 AND SENTINEL-1 RADAR DATA FOR SOIL MOISTURE RETRIEVAL 13
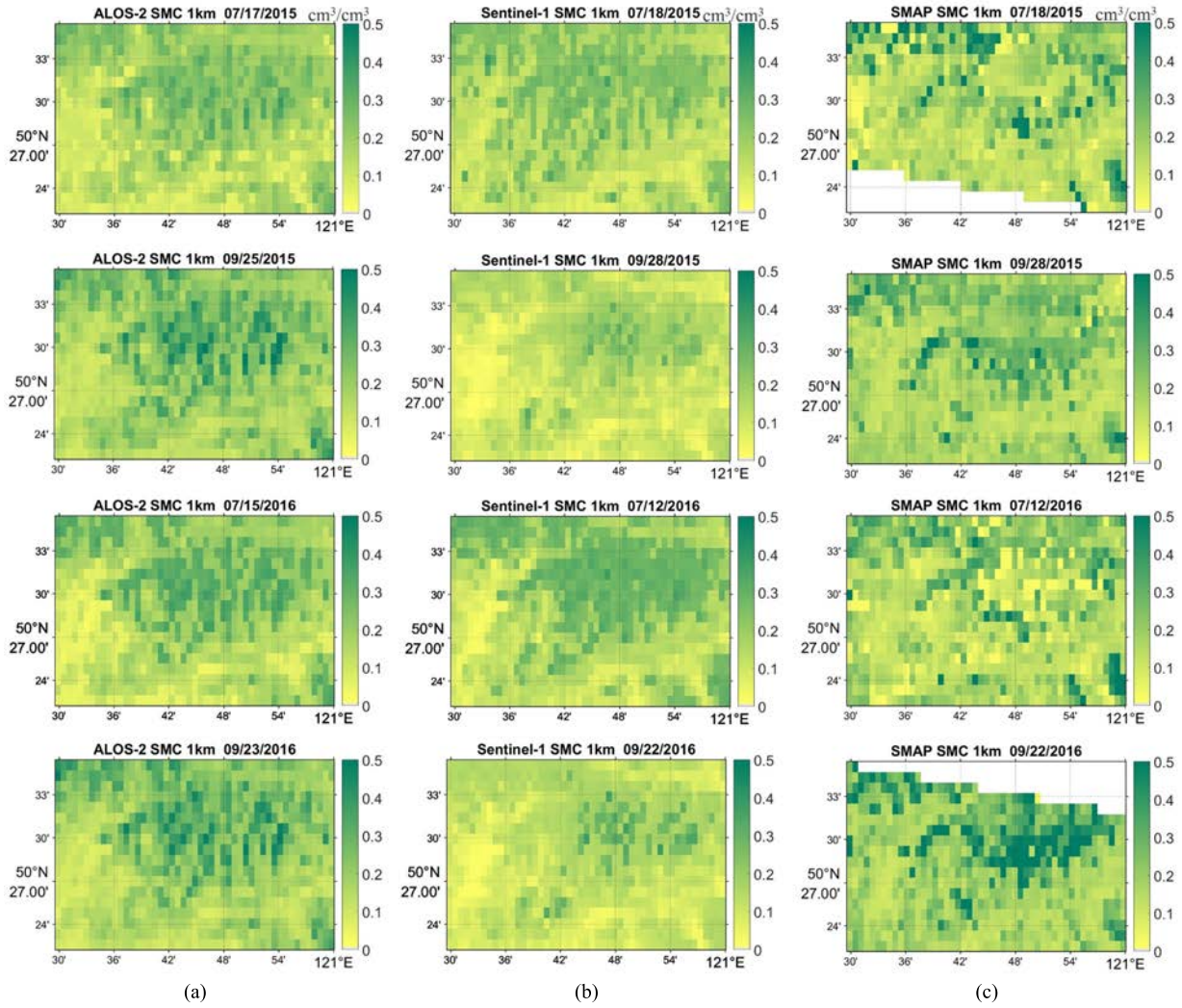

Fig. 15. Spatial distribution of (a) left column: ALOS-2 SMC, (b) middle column: Sentinel-1 SMC, and (c) right column: SMAP SMC at 1-km resolution.

TABLE VIII
ERROR METRICS FOR SENTINEL-1 AND ALOS-2 SMC RETRIEVAL

Parameter	Date	R	RMSE (cm³/cm³)	Bias (cm³/cm³)
Sentinel-1 vs. SMAP SMC	Jul. 18, 2015	0.29	0.045	0.013
	Sep. 28, 2015	0.37	0.053	-0.078
	Jul. 12, 2016	0.30	0.064	0.016
	Sep. 22, 2016	0.47	0.049	-0.120
ALOS-2 vs. SMAP SMC	Jul. 17, 2015	0.33	0.061	0.008
	Sep. 25, 2015	0.40	0.078	0.012
	Jul. 15, 2016	0.27	0.062	0.007
	Sep. 23, 2016	0.52	0.080	-0.033

Fig. 14(a), (b), (e), and (f)]. This finding is due to the vegetation growing ($0.4 <$ NDVI < 0.87) in July and the vegetation drying ($0.3 <$ NDVI < 0.72) in September, and consequently, the effect of vegetation on the SMC retrieval is reduced in September. The RMSE of Sentinel-1 is lower than that of ALOS-2 (see Table VIII). The main reason is that the overpass time of Sentinel-1 is closer to SMAP L2 than that of ALOS-2. In fact, the overpass time difference

will affect the validation results, especially in one to three days. In addition, the time-series variation of *in situ* SMC shows that SMC observations in September are wetter than in July from 2015 to 2016 [3]. This is because the rainfall is more frequent in September than July (see Fig. 11). In July, there is less precipitation, and the soil moisture is relatively dry. Therefore, the RMSE is also generally lower in July than September in particularly for ALOS-2. Sentinel-1 and ALOS have a lot of saturated soil moisture at high-vegetation areas, which is different from SMAP SMC (in Fig. 15). SMAP L2 SMC combines the C-band radar measurements with high-resolution spatial details and the advantages of L-band radiometer measurements that are sensitive to surface SMC [80]. It is the main difference between ALOS-2 (L-band SAR) and Sentinel-1 (C-band SAR). Besides, vegetation correction methods are different in soil moisture retrieval. NDVI was used for vegetation correction in the ALOS-2, Sentinel-1, and SMAP SMC retrieval algorithm. The main difference is that the vegetation contributions from the foliage and stem components are taken into consideration in the SMAP algorithm [81]. In order to distinguish the different effects of the vegetation

correction methods, the vegetation transmissivity at L-band frequencies (SMAP) was calculated by equation (8) in [81] from the vegetation opacity in SMAP L2 SP soil moisture product, and the vegetation transmissivity at C-band and L-band SAR was calculated by (3) in this work. The range of vegetation transmissivity at SMAP L-band (0.25~0.92) is wider than that of Sentinel-1 C-band (0.45~0.84) and ALOS-2 L-band (0.52~0.94), which may be the main reason for that the range of SMAP SMC is wider than Sentinel-1 and ALOS-2 SMC and has less saturation value in this work.

From the spatial distributions of the ALOS-2, Sentinel-1, and SMAP SMC (in Fig. 15), there are some missing data for the SMAP L2 SMC in the studied area [in Fig. 15(c)] due to the difference in swath width between SMAP and Sentinel-1. ALOS-2, Sentinel-1, and SMAP SMC are usually higher in high vegetation (forest) than in low-vegetation (grass, crop, and shrub) areas, which corresponds to the land classification map. Perhaps, the presence of well-developed vegetation over the soil contributes to keeping more water content due to the reduced surface evaporation [82]. The spatial distribution of SMC shows that the Sentinel-1 SMC is usually lower than that of the SMAP in September [see Fig. 15(b) and (c)], and the ALOS-2 SMC value is closer to the SMAP SMC, except for some forest areas [see Fig. 15(a) and (c)]. SMAP and ALOS-2 SMC are higher in September than in July from 2015 to 2016, which is consistent with the time-series variation of *in situ* SMC [3]. The land surface temperature in July is higher than in September [3], and surface evapotranspiration increases with the increase in the surface temperature, which leads to surface drying. However, Sentinel-1 SMC is lower in September than in July, which indicates that SMAP and ALOS-2 SMC are more consistent with the measured SMC than Sentinel-1, and the correlation between the ALOS-2 SMC retrievals and SMAP is higher than the correlation from Sentinel-1 in September [see Fig. 14(c), (d), (g), and (h)]. Due to the high attenuation effect of the dense vegetation cover (NDVI > 0.7), the C-band SAR signal becomes insensitive to the surface SMC, whereas the L-band SAR signal is still sensitive to the SMC [51].

Overall, the spatial distribution of ALOS-2 SMC is closer to the SMAP SMC than Sentinel-1. SMAP L2 active and passive SMC product combines the advantages of radiometer measurements and radar measurements, showing an accuracy of ~0.075 cm^3/cm^3 in the Genhe area. If users want to use SMC products with a coarser spatial resolution (i.e., ≥1 km), they can refer to SMAP L2 active and passive SMC products. If users need higher spatial resolution SMC data (i.e., <1 km), L-band SAR is the better choice for SMC retrieval in an agroforestry area.

V. CONCLUSION

In this work, the ANN algorithm was used to investigate the potential of Sentinel-1 (C-band) and ALOS-2 (L-band) SAR for SMC retrieval in agroforestry areas. Based on the parameters analysis, the copolarization backscattering coefficient (VV or HH), the incidence angle, NDVI, and SMC from the simulated databases are used for ANN training and testing. According to the result of ANN training and

testing, the ALOS-2 and Sentinel-1 SMC at 30-m resolution were obtained from the ALOS-2 and Sentinel-1 SAR backscatter, LIA, and NDVI, respectively. Subsequently, both the ground measured data and SMAP L2 active and passive SMC data were used to intercompare the Sentinel-1 and ALOS-2 SMC, respectively. The results of the comparison between the Sentinel-1, ALOS-2 SMC, and the measured SMC show that Sentinel-1 and ALOS-2 can provide SMC estimates with high accuracy over low-vegetation soils (crop, grass, and shrub). The accuracy of the ALOS-2 SMC retrieval over high-vegetation soils (forest) is higher than that of Sentinel-1. This finding occurs because of the higher frequency of the C-band, which is less able to penetrate the dense vegetation surfaces; thus, the backscatter received by the SAR contains a negligible SMC contribution under these conditions. The results of the intercomparison between the ANN SMC retrievals and the SMAP L2 SMC product show that the correlations between Sentinel-1, ALOS-2 SMC, and SMAP SMC when the vegetation is drying in September are higher than when the vegetation is growing in July. The RMSE between Sentinel-1 SMC and SMAP SMC is lower than that of ALOS-2 because the overpass time of SMAP L2 is close to Sentinel-1. The influence of LIA on the SMC retrieval shows that the incidence angle (20°~50°) has little effect on the accuracy of SMC retrievals, and C-band and L-band SMC retrievals have higher RMSE at low incidence angle (10°) and high incidence angle (60°). The influence of rainfall on the SMC retrieval shows that the Sentinel-1 and ALOS-2 SMC have a good response to the rainfall events.

ALOS-2 L-band SAR appears to have more potential than the Sentinel-1 C-band SAR to estimate SMC in agroforestry areas. The SMC retrieval from the Sentinel-1 C-band SAR in high-vegetation areas is unreliable, with higher errors (0.14 cm^3/cm^3) due to the limited penetration of the C-band and the consequent significant effect of vegetation on the SMC sensitivity, and the large incidence angles also affect the accuracy of SMC retrievals. However, the C-band SAR has a high potential for SMC retrieval in the crop, grass, and shrub land (low-vegetation areas). The limitations of the ground measured SMC data produce more uncertainty for the validation of the proposed algorithm. The SMAP L2 SMC product has been used as a reference (not a truth value) to intercompare the Sentinel-1 and ALOS-2 SMC estimates; it cannot completely substitute for *in situ* data, which introduces some errors and affects the comparison results.

ANN has the power to retrieve the complex, dynamic, and nonlinear patterns from the data, but it is "black boxes," and the user has no control, except providing the input data. This is the limitation of the ANN algorithm, which leads to the uncertainty of the SMC estimates. Although the soil moisture maps at 30-m resolution were obtained in this work, it still has a few speckles in the soil moisture maps. Therefore, effective removal of speckles in SAR images is also an issue that needs to be considered in future soil moisture retrieval at the meter scale. Meanwhile, semiempirical and electromagnetic vegetation models are used to build a synthetic database while ignoring the multiple scattering effects between canopy layers and NDVI as the vegetation's descriptor in WCM is

easily saturated in forest areas, which could produce some negative impacts on the retrieval results. SMC retrieval in dense and high vegetation is always a key but challenging task, and this work represents only a beginning. In future work, we will consider the previously mentioned factors, by collecting more *in situ* data and SAR images to investigate the potential of the L-band and C-band SAR sensors in estimating the SMC. Moreover, it is advisable to adopt an optimized vegetation correction method to improve the accuracy of the SMC retrievals and obtain high-resolution SMC maps.

ACKNOWLEDGMENT

REFERENCES

[1] J. Shi, J. Wang, A. Y. Hsu, P. E. O'Neill, and E. T. Engman, "Estimation of bare surface soil moisture and surface roughness parameter using L-band SAR image data," *IEEE Trans. Geosci. Remote Sens.*, vol. 35, no. 5, pp. 1254–1266, Sep. 1997.

[2] J. Peng *et al.*, "A roadmap for high-resolution satellite soil moisture applications—Confronting product characteristics with user requirements," *Remote Sens. Environ.*, vol. 252, Jan. 2021, Art. no. 112162.

[3] H. Cui *et al.*, "Evaluation and analysis of AMSR-2, SMOS, and SMAP soil moisture products in the Genhe area of China," *J. Geophys. Res., Atmos.*, vol. 122, no. 16, pp. 8650–8666, Aug. 2017.

[4] W. W. Verstraeten, F. Veroustraete, C. J. van der Sande, I. Grootaers, and J. Feyen, "Soil moisture retrieval using thermal inertia, determined with visible and thermal spaceborne data, validated for European forests," *Remote Sens. Environ.*, vol. 101, no. 3, pp. 299–314, Apr. 2006.

[5] R. D. de Roo, Y. Du, F. T. Ulaby, and M. C. Dobson, "A semi-empirical backscattering model at L-band and C-band for a soybean canopy with soil moisture inversion," *IEEE Trans. Geosci. Remote Sens.*, vol. 39, no. 4, pp. 864–872, Apr. 2001.

[6] A. Balenzano, F. Mattia, G. Satalino, and M. W. J. Davidson, "Dense temporal series of C- and L-band SAR data for soil moisture retrieval over agricultural crops," *IEEE J. Sel. Topics Appl. Earth Observ. Remote Sens.*, vol. 4, no. 2, pp. 439–450, Jun. 2011.

[7] A. Tabatabaeenejad, M. Burgin, X. Duan, and M. Moghaddam, "P-band radar retrieval of subsurface soil moisture profile as a second-order polynomial: First AirMOSS results," *IEEE Trans. Geosci. Remote Sens.*, vol. 53, no. 2, pp. 645–658, Feb. 2015.

[8] G. Macelloni *et al.*, "The SIR-C/X-SAR experiment on montespertoli: Sensitivity to hydrological parameters," *Int. J. Remote Sens.*, vol. 20, no. 13, pp. 2597–2612, Jan. 1999.

[9] M. E. Hajj *et al.*, "Soil moisture retrieval over irrigated grassland using X-band SAR data," *Remote Sens. Environ.*, vol. 176, pp. 202–218, Apr. 2016.

[10] Q. Gao, M. Zribi, M. Escorihuela, and N. Baghdadi, "Synergetic use of Sentinel-1 and Sentinel-2 data for soil moisture mapping at 100 m resolution," *Sensors*, vol. 17, no. 9, p. 1966, Aug. 2017.

[11] A. Amazirh *et al.*, "Retrieving surface soil moisture at high spatio-temporal resolution from a synergy between Sentinel-1 radar and landsat thermal data: A study case over bare soil," *Remote Sens. Environ.*, vol. 211, pp. 321–337, Jun. 2018.

[12] J. Ezzahar *et al.*, "Evaluation of backscattering models and support vector machine for the retrieval of bare soil moisture from Sentinel-1 data," *Remote Sens.*, vol. 12, no. 1, p. 72, Dec. 2019.

[13] M. Foucras, M. Zribi, C. Albergel, N. Baghdadi, J.-C. Calvet, and T. Pellarin, "Estimating 500-m resolution soil moisture using Sentinel-1 and optical data synergy," *Water*, vol. 12, no. 3, p. 866, Mar. 2020.

[14] B. Bauer-Marschallinger *et al.*, "Toward global soil moisture monitoring with Sentinel-1: Harnessing assets and overcoming obstacles," *IEEE Trans. Geosci. Remote Sens.*, vol. 57, no. 1, pp. 520–539, Jan. 2019.

[15] M. Zribi *et al.*, "Analysis of L-band SAR data for soil moisture estimations over agricultural areas in the tropics," *Remote Sens.*, vol. 11, no. 9, p. 1122, May 2019.

[16] Y. Izumi *et al.*, "Potential of soil moisture retrieval for tropical peatlands in Indonesia using ALOS-2 L-band full-polarimetric SAR data," *Int. J. Remote Sens.*, vol. 40, no. 15, pp. 5938–5956, Aug. 2019.

[17] A. K. Fung and K. S. Chen, "An update on the IEM surface backscattering model," *IEEE Geosci. Remote Sens. Lett.*, vol. 1, no. 2, pp. 75–77, Apr. 2004.

[18] T.-D. Wu and K.-S. Chen, "A reappraisal of the validity of the IEM model for backscattering from rough surfaces," *IEEE Trans. Geosci. Remote Sens.*, vol. 42, no. 4, pp. 743–753, Apr. 2004.

[19] Y. Oh, K. Sarabandi, and F. T. Ulaby, "An empirical model and an inversion technique for radar scattering from bare soil surfaces," *IEEE Trans. Geosci. Remote Sens.*, vol. 30, no. 2, pp. 370–381, Mar. 1992.

[20] E. P. W. Attema and F. T. Ulaby, "Vegetation modeled as a water cloud," *Radio Sci.*, vol. 13, no. 2, pp. 357–364, Mar. 1978.

[21] F. T. Ulaby, K. Sarabandi, K. McDONALD, M. Whitt, and M. C. Dobson, "Michigan microwave canopy scattering model," *Int. J. Remote Sens.*, vol. 11, no. 7, pp. 1223–1253, Jul. 1990.

[22] S. Paloscia, S. Pettinato, E. Santi, C. Notarnicola, L. Pasolli, and A. Reppucci, "Soil moisture mapping using Sentinel-1 images: Algorithm and preliminary validation," *Remote Sens. Environ.*, vol. 134, pp. 234–248, Jul. 2013.

[23] M. E. Hajj, N. Baghdadi, M. Zribi, and H. Bazzi, "Synergic use of Sentinel-1 and Sentinel-2 images for operational soil moisture mapping at high spatial resolution over agricultural areas," *Remote Sens.*, vol. 9, no. 12, p. 1292, Dec. 2017.

[24] S. Paloscia, P. Pampaloni, S. Pettinato, and E. Santi, "A comparison of algorithms for retrieving soil moisture from ENVISAT/ASAR images," *IEEE Trans. Geosci. Remote Sens.*, vol. 46, no. 10, pp. 3274–3284, Oct. 2008.

[25] M. Zribi *et al.*, "Soil surface moisture estimation over a semi-arid region using ENVISAT ASAR radar data for soil evaporation evaluation," *Hydrol. Earth Syst. Sci.*, vol. 15, no. 1, pp. 345–358, Jan. 2011.

[26] W. Wagner, G. Lemoine, M. Borgeaud, and H. Rott, "A study of vegetation cover effects on ERS scatterometer data," *IEEE Trans. Geosci. Remote Sens.*, vol. 37, no. 2, pp. 938–948, Mar. 1999.

[27] H. R. Mirsoleimani *et al.*, "Bare soil surface moisture retrieval from Sentinel-1 SAR data based on the calibrated IEM and DuBois models using neural networks," *Sensors*, vol. 19, no. 14, pp. 1–12, Jul. 2019.

[28] S.-B. Kim, L. Tsang, J. T. Johnson, S. Huang, J. J. van Zyl, and E. G. Njoku, "Soil moisture retrieval using time-series radar observations over bare surfaces," *IEEE Trans. Geosci. Remote Sens.*, vol. 50, no. 5, pp. 1853–1863, May 2012.

[29] W. Wagner and K. Scipal, "Large-scale soil moisture mapping in Western Africa using the ERS scatterometer," *IEEE Trans. Geosci. Remote Sens.*, vol. 38, no. 4, pp. 1777–1782, Jul. 2000.

[30] M. Zribi and M. Dechambre, "A new empirical model to retrieve soil moisture and roughness from C-band radar data," *Remote Sens. Environ.*, vol. 84, no. 1, pp. 42–52, Jan. 2003.

[31] F. Mattia, G. Satalino, L. Dente, and G. Pasquariello, "Using a priori information to improve soil moisture retrieval from ENVISAT ASAR AP data in semiarid regions," *IEEE Trans. Geosci. Remote Sens.*, vol. 44, no. 4, pp. 900–912, Apr. 2006.

[32] Y. Zeng *et al.*, "A radiative transfer model for heterogeneous agro-forestry scenarios," *IEEE Trans. Geosci. Remote Sens.*, vol. 54, no. 8, pp. 4613–4628, Aug. 2016.

[33] E. Santi, S. Paloscia, S. Pettinato, C. Notarnicola, L. Pasolli, and A. Pistocchi, "Comparison between SAR soil moisture estimates and hydrological model simulations over the Scrivia test site," *Remote Sens.*, vol. 5, no. 10, pp. 4961–4976, Oct. 2013.

[34] A. Hachani, M. Ouessar, S. Paloscia, E. Santi, and S. Pettinato, "Soil moisture retrieval from Sentinel-1 acquisitions in an arid environment in Tunisia: Application of artificial neural networks techniques," *Int. J. Remote Sens.*, vol. 40, no. 24, pp. 9159–9180, Dec. 2019.

[35] K. Jia *et al.*, "Global land surface fractional vegetation cover estimation using general regression neural networks from MODIS surface reflectance," *IEEE Trans. Geosci. Remote Sens.*, vol. 53, no. 9, pp. 4787–4796, Sep. 2015.

This article has been accepted for inclusion in a future issue of this journal. Content is final as presented, with the exception of pagination.

16   IEEE TRANSACTIONS ON GEOSCIENCE AND REMOTE SENSING

[36] Z. Xiao *et al.*, "Use of general regression neural networks for generating the GLASS leaf area index product from time-series MODIS surface reflectance," *IEEE Trans. Geosci. Remote Sens.*, vol. 52, no. 1, pp. 209–223, Jan. 2014.

[37] E. Santi, M. Dabboor, S. Pettinato, and S. Paloscia, "Combining machine learning and compact polarimetry for estimating soil moisture from C-band SAR data," *Remote Sens.*, vol. 11, no. 20, p. 2451, Oct. 2019.

[38] M. Zribi, N. Baghdadi, S. Bousbih, M. El-Hajj, and Q. Gao, "Surface moisture and irrigation mapping at agricultural field scale using the synergy Sentinel-1/Sentinel-2 data," *ISPRS-Int. Arch. Photogramm., Remote Sens. Spatial Inf. Sci.*, vol. 3/W6, pp. 357–361, Jul. 2019.

[39] L. Jiang *et al.*, "*In situ* soil moisture and temperature network in Genhe watershed and Saihanba area in China," *Data Brief*, vol. 31, Aug. 2020, Art. no. 105693.

[40] X. Tian *et al.*, "The complicate observations and multi-parameter land information constructions on allied telemetry experiment (COMPLI-CATE)," *PLoS ONE*, vol. 10, no. 9, Sep. 2015, Art. no. e0137545.

[41] R. Torres *et al.*, "GMES Sentinel-1 mission," *Remote Sens. Environ.*, vol. 120, pp. 9–24, May 2012.

[42] Y. Kankaku, S. Suzuki, and Y. Osawa, "ALOS-2 mission and development status," in *Proc. IEEE Int. Geosci. Remote Sens. Symp. (IGARSS)*, Jul. 2013, pp. 2396–2399.

[43] S. Suzuki, Y. Kankaku, and Y. Osawa, "Development status of PALSAR-2 onboard ALOS-2," *Proc. SPIE*, vol. 8176, Oct. 2011, Art. no. 81760Q.

[44] Q. Wang *et al.*, "Fusion of landsat 8 OLI and Sentinel-2 MSI data," *IEEE Trans. Geosci. Remote Sens.*, vol. 55, no. 7, pp. 3885–3899, Jul. 2017.

[45] M. Drusch *et al.*, "Sentinel-2: ESA's optical high-resolution mission for GMES operational services," *Remote Sens. Environ.*, vol. 120, pp. 25–36, May 2012.

[46] T. R. Loveland and J. R. Irons, "Landsat 8: The plans, the reality, and the legacy," *Remote Sens. Environ.*, vol. 185, pp. 1–6, Nov. 2016.

[47] J. Chen, Y. Ban, and S. Li, "China: Open access to Earth land-cover map," *Nature*, vol. 514, no. 7523, p. 434, Oct. 2014.

[48] M. E. Hajj, N. Baghdadi, and M. Zribi, "Comparative analysis of the accuracy of surface soil moisture estimation from the C- and L-bands," *Int. J. Appl. Earth Observ. Geoinf.*, vol. 82, Oct. 2019, Art. no. 101888.

[49] S. C. M. Brown, S. Quegan, K. Morrison, J. C. Bennett, and G. Cookmartin, "High-resolution measurements of scattering in wheat canopies-implications for crop parameter retrieval," *IEEE Trans. Geosci. Remote Sens.*, vol. 41, no. 7, pp. 1602–1610, Jul. 2003.

[50] F. D. Frate *et al.*, "Wheat cycle monitoring using radar data and a neural network trained by a model," *IEEE Trans. Geosci. Remote Sens.*, vol. 42, no. 1, pp. 35–44, Jan. 2004.

[51] M. E. Hajj, N. Baghdadi, H. Bazzi, and M. Zribi, "Penetration analysis of SAR signals in the C and L bands for wheat, maize, and grasslands," *Remote Sens.*, vol. 11, no. 1, p. 31, Dec. 2018.

[52] F. Ulaby, "Radar response to vegetation," *IEEE Trans. Antennas Propag.*, vol. AP-23, no. 1, pp. 36–45, Jan. 1975.

[53] F. T. Ulaby, G. A. Bradley, and M. C. Dobson, "Microwave backscatter dependence on surface roughness, soil moisture, and soil texture: Part II-vegetation-covered soil," *IEEE Trans. Geosci. Electron.*, vol. GE-17, no. 2, pp. 33–40, Apr. 1979.

[54] D. Alexakis, F.-D. Mexis, A.-E. Vozinaki, I. Daliakopoulos, and I. Tsanis, "Soil moisture content estimation based on Sentinel-1 and auxiliary Earth observation products. A hydrological approach," *Sensors*, vol. 17, no. 6, p. 1455, Jun. 2017.

[55] E. Santi, S. Paloscia, S. Pettinato, and G. Fontanelli, "Application of artificial neural networks for the soil moisture retrieval from active and passive microwave spaceborne sensors," *Int. J. Appl. Earth Observ. Geoinf.*, vol. 48, pp. 61–73, Jun. 2016.

[56] F. T. Ulaby, C. T. Allen, G. Eger, and E. Kanemasu, "Relating the microwave backscattering coefficient to leaf area index," *Remote Sens. Environ.*, vol. 14, nos. 1–3, pp. 113–133, Jan. 1984.

[57] R. Bindlish and A. P. Barros, "Parameterization of vegetation backscatter in radar-based, soil moisture estimation," *Remote Sens. Environ.*, vol. 76, no. 1, pp. 130–137, Apr. 2001.

[58] N. Baghdadi, M. E. Hajj, M. Zribi, and S. Bousbih, "Calibration of the water cloud model at C-band for winter crop fields and grasslands," *Remote Sens.*, vol. 9, no. 9, p. 969, Sep. 2017.

[59] A. J. Graham and R. Harris, "Extracting biophysical parameters from remotely sensed radar data: A review of the water cloud model," *Prog. Phys. Geography, Earth Environ.*, vol. 27, no. 2, pp. 217–229, Jun. 2003.

[60] J. Zeng, K.-S. Chen, H. Bi, T. Zhao, and X. Yang, "A comprehensive analysis of rough soil surface scattering and emission predicted by AIEM with comparison to numerical simulations and experimental measurements," *IEEE Trans. Geosci. Remote Sens.*, vol. 55, no. 3, pp. 1696–1708, Mar. 2017.

[61] Y. Oh, K. Sarabandi, and F. T. Ulaby, "Semi-empirical model of the ensemble-averaged differential Mueller matrix for microwave backscattering from bare soil surfaces," *IEEE Trans. Geosci. Remote Sens.*, vol. 40, no. 6, pp. 1348–1355, Jun. 2002.

[62] J. A. Nelder and R. Mead, "A simplex-method for function minimization," *Comput. J.*, vol. 7, no. 4, pp. 308–313, 1965.

[63] A. Sekertekin, A. M. Marangoz, and S. Abdikan, "ALOS-2 and Sentinel-1 SAR data sensitivity analysis to surface soil moisture over bare and vegetated agricultural fields," *Comput. Electron. Agricult.*, vol. 171, Apr. 2020, Art. no. 105303.

[64] F. T. Ulaby, R. K. Moore, and A. K. Fung, *Microwave Remote Sensing: Active and Passive*, vol. 3. Dedham, MA, USA: Artech House, 1986.

[65] N. Baghdadi *et al.*, "Analysis of TerraSAR-X data and their sensitivity to soil surface parameters over bare agricultural fields," *Remote Sens. Environ.*, vol. 112, no. 12, pp. 4370–4379, 2008.

[66] T. L. Toan, H. Laur, E. Mougin, and A. Lopes, "Multitemporal and dual-polarization observations of agricultural vegetation covers by X-band SAR images," *IEEE Trans. Geosci. Remote Sens.*, vol. 27, no. 6, pp. 709–718, Nov. 1989.

[67] M. C. Dobson and F. T. Ulaby, "Active microwave soil moisture research," *IEEE Trans. Geosci. Remote Sens.*, vol. GRS-24, no. 1, pp. 23–36, Jan. 1986.

[68] Y. Wang, J. L. Day, and F. W. Davis, "Sensitivity of modeled C- and L-band radar backscatter to ground surface parameters in loblolly pine forest," *Remote Sens. Environ.*, vol. 66, no. 3, pp. 331–342, 1998.

[69] H. S. Srivastava, P. Patel, Y. Sharma, and R. R. Navalgund, "Large-area soil moisture estimation using multi-incidence-angle RADARSAT-1 SAR data," *IEEE Trans. Geosci. Remote Sens.*, vol. 47, no. 8, pp. 2528–2535, Aug. 2009.

[70] F. Mattia *et al.*, "The effect of surface roughness on multifrequency polarimetric SAR data," *IEEE Trans. Geosci. Remote Sens.*, vol. 35, no. 4, pp. 954–966, Jul. 1997.

[71] M. Zribi, A. Gorrab, N. Baghdadi, Z. Lili-Chabaane, and B. Mougenot, "Influence of radar frequency on the relationship between bare surface soil moisture vertical profile and radar backscatter," *IEEE Geosci. Remote Sens. Lett.*, vol. 11, no. 4, pp. 848–852, Apr. 2014.

[72] J. F. Paris, "Radar backscattering properties of corn and soybeans at frequencies of 1.6, 4.75, and 13.3 GHz," *IEEE Trans. Geosci. Remote Sens.*, vol. GRS-21, no. 3, pp. 392–400, Jul. 1983.

[73] G. Sun, D. S. Simonett, and A. H. Strahler, "A radar backscatter model for discontinuous coniferous forests," *IEEE Trans. Geosci. Remote Sens.*, vol. 29, no. 4, pp. 639–650, Jul. 1991.

[74] M. Miernecki *et al.*, "Comparison of SMOS and SMAP soil moisture retrieval approaches using tower-based radiometer data over a vineyard field," *Remote Sens. Environ.*, vol. 154, pp. 89–101, Nov. 2014.

[75] T. J. Jackson *et al.*, "Validation of soil moisture and ocean salinity (SMOS) soil moisture over watershed networks in the U.S." *IEEE Trans. Geosci. Remote Sens.*, vol. 50, no. 5, pp. 1530–1543, May 2012.

[76] A. Loew, M. Schwank, and F. Schlenz, "Assimilation of an L-band microwave soil moisture proxy to compensate for uncertainties in precipitation data," *IEEE Trans. Geosci. Remote Sens.*, vol. 47, no. 8, pp. 2606–2616, Aug. 2009.

[77] C. Román-Cascón *et al.*, "Can we use satellite-based soil-moisture products at high resolution to investigate land-use differences and Land–Atmosphere interactions? A case study in the savanna," *Remote Sens.*, vol. 12, no. 11, p. 1701, May 2020.

[78] T. Chen, R. A. M. de Jeu, Y. Y. Liu, G. R. van der Werf, and A. J. Dolman, "Using satellite based soil moisture to quantify the water driven variability in NDVI: A case study over mainland Australia," *Remote Sens. Environ.*, vol. 140, pp. 330–338, Jan. 2014.

[79] S.-W. Chen, "SAR image speckle filtering with context covariance matrix formulation and similarity test," *IEEE Trans. Image Process.*, vol. 29, pp. 6641–6654, 2020.

[80] N. N. Das *et al.*, "The SMAP and copernicus sentinel 1A/B microwave active-passive high resolution surface soil moisture product," *Remote Sens. Environ.*, vol. 233, Nov. 2019, Art. no. 111380.

[81] P. O'Neill *et al.*, "Soil moisture active passive (SMAP): Algorithm theoretical basis document level 2 & 3 soil moisture (Passive) data products," SMAP Sci. Document, Revision F, Jet Propuls. Lab., California Inst. Technol., Pasadena, CA, USA, Tech. Rep. JPL D-66480, 2020.

[82] M. S. Yee, J. P. Walker, A. Monerris, C. Rüdiger, and T. J. Jackson, "On the identification of representative *in situ* soil moisture monitoring stations for the validation of SMAP soil moisture products in Australia," *J. Hydrol.*, vol. 537, pp. 367–381, Jun. 2016.

Huizhen Cui received the Ph.D. degree in cartography and geographic information system from the Faculty of Geographical Science, Beijing Normal University, Beijing, China, in July 2019.

From 2017 to 2018, she was a Visiting Ph.D. Student with the Institute of Applied Physics, National Research Council (IFAC-CNR), Florence, Italy. She holds a post-doctoral position at the College of Life Sciences, Beijing Normal University. Her research interests include microwave remote sensing of soil moisture and microwave emission and scattering modeling of the land surface.

Lingmei Jiang (Member, IEEE) received the Ph.D. degree in geography from Beijing Normal University, Beijing, China, in July 2005.

She is a Professor with the Faculty of Geographical Science, Beijing Normal University. She has authored/coauthored over 150 scientific publications. Her research interests include microwave emission/scattering modeling of the land surface, passive microwave remote sensing of snow water equivalent and soil moisture, surface freeze/thaw state, and remote sensing data assimilated into the land surface model.

Dr. Jiang has been awarded the Shi Yafeng Prize for Young Scientists in Cryosphere and Environment in 2018.

Simonetta Paloscia (Fellow, IEEE) has been with the National Research Council (CNR), Florence, Italy, since 1984. Since 2004, she has been scientific responsible for the Microwave Remote Sensing Group, Institute of Applied Physics (IFAC)-CNR, and the research line "Microwave Remote Sensing of Natural Surfaces," in the EO Project of CNR. In 2010, she was nominated for the Research Director at CNR. She is the author or a coauthor of more than 100 works published in international journals and books and more than 200 articles published on proceedings of international meetings. Her research focuses on the study of microwave emission and scattering of soil (bare and snow-covered) and vegetation.

Dr. Paloscia was a member of organizing and steering committees of international meetings (Specialist Meeting on Microwave Radiometry and International Geoscience and Remote Sensing Symposium). She is a member of the Soil Moisture Active Passive (SMAP) JPL/NASA Science Team. She is also a member of the Permanent Steering Committee of MicroRad Meeting and the General Co-Chair of the MicroRad 1999 and 2008 and URSI-F 2010 Meetings organized in Florence. She has been a URSI Fellow since 2020. She was a PI and a Co-I of many national and international projects [the Italian Space Agency (ASI), the European Community (EC), the European Space Agency (ESA), and the Japan Aerospace and Exploration Agency (JAXA)]. Since 1996, she has been a Principal Investigator in the JAXA Science Team of AQUA/AMSR-E and GCOM/AMSR-2 for algorithms' development of soil moisture and vegetation biomass retrieval. She was the Vice-Chair and the Chair of the URSI Commission F from 2011 to 2017. She is an Associate Editor of the *International Journal of Remote Sensing*, IEEE JOURNAL OF SELECTED TOPICS IN APPLIED EARTH OBSERVATIONS AND REMOTE SENSING (IEEE J-STARS), and *European Journal of Remote Sensing*.

Emanuele Santi (Senior Member, IEEE) received the M.S. degree in electronic engineering from the University of Florence, Florence, Italy, in 1997, and the Ph.D. degree in Earth's remote sensing techniques from the University of Basilicata, Potenza, Italy, in 2005.

Since 1998, he has been a Researcher with the Microwave Remote Sensing Group, Institute of Applied Physics, National Research Council, Florence. He has been involved in many national and international projects funded by the Italian Space Agency (ASI), the European Community (EC), the European Space Agency (ESA), and the Japanese Aerospace Exploration Agency (JAXA), acting as a Team Leader, a WP Leader, and a Co-Investigator. He has authored or coauthored 158 articles, published on ISI journals and books and conference proceedings (source: Scopus). His research interests include the development and validation of models and statistical inversion algorithms for estimating the geophysical parameters of soil, sea, snow, and vegetation from microwave emission and scattering.

Dr. Santi is a member of the "Centro di Telerilevamento a Microonde" (Microwave Remote Sensing Center). In 2018, he won the IEEE GRSS J-STARS Prize Paper Award for the best paper published on IEEE JOURNAL OF SELECTED TOPICS IN APPLIED EARTH OBSERVATIONS AND REMOTE SENSING (IEEE J-STARS) in 2017. He is also the Conference Chair of the SPIE Europe Remote Sensing Conference (RS-106).

Simone Pettinato (Member, IEEE) received the M.S. degree in telecommunications engineering from the University of Florence, Florence, Italy, in 2002, and the Ph.D. degree in methods and technologies for environmental monitoring from the University of Basilicata, Potenza, Italy, in 2007.

Since 2003, he has been a Scientist with the Microwave Remote Sensing Group, Institute of Applied Physics, National Research Council (IFAC-CNR), Florence. He has participated, as a co-investigator, in different national and international scientific projects funded by the European Community and European and Italian space agencies [the European Space Agency (ESA) and the Italian Space Agency (ASI)]. From 2009 to 2012, he was involved in three Antarctic expeditions in the framework of the DOMEX-2, DOMEX-3, and GPS-SIDS projects. He is the author or a coauthor of more than 100 articles published in international peer-reviewed journals and conference proceedings. His research focuses on the investigation of the natural surfaces by means of active and passive microwave sensors in order to retrieve information on geophysical parameters related to the hydrological cycle (soil moisture, snow, and vegetation).

Jian Wang received the B.S. degree from Yanshan University, Qinhuangdao, China, in 2016. She is pursuing the Ph.D. degree in cartography and geography information system with Beijing Normal University, Beijing, China.

Her research interests include microwave emission and scattering modeling of soil and monitoring surface freeze/thaw state with microwave remote sensing.

Xiyao Fang received the B.S. degree in geographic information science from Jilin University, Changchun, China, in 2019. She is pursuing the master's degree in cartography and geographic information system with Beijing Normal University, Beijing, China.

Her research interest includes microwave remote sensing of soil moisture.
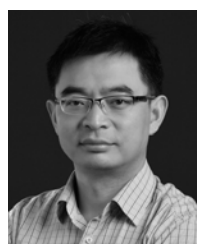
Wanjin Liao received the Ph.D. degree in ecology from Beijing Normal University, Beijing, China, in 2005.

He is a Professor with the College of Life Sciences, Beijing Normal University, where he is the Chair of the Department of Ecology. His research interests mainly include ecology and evolution of plant reproduction, maintenance of biodiversity, and coevolution of interspecific interactions.